

# Chapter 13

## Testing Gravity and Predictions Beyond the Standard Model at Short Distances: The Casimir Effect

Galina L. Klimchitskaya and Vladimir M. Mostepanenko

13.1	Introduction: Gravity, the Standard Model and Beyond .....	2
13.2	Electromagnetic Casimir Force and the Quantum Vacuum .....	4
13.3	Testing the Power-Type Corrections to Newtonian Gravity from the Casimir Effect ..	8
13.4	Testing the Yukawa-Type Corrections to Newtonian Gravity from the Casimir Effect	12
13.5	Dark Matter, Dark Energy and Their Hypothetical Constituents .....	20
13.6	Constraining Dark Matter Particles from the Casimir Effect .....	22
13.7	Could the Casimir Effect be Used For Testing Spin-Dependent Interactions? .....	27
13.8	Constraining Dark Energy Particles from the Casimir Effect .....	29
13.9	Outlook .....	31
	References .....	33

**Abstract** The Standard Model of elementary particles and their interactions does not include the gravitational interaction and faces problems in understanding of the dark matter, dark energy, strong CP violation etc. In continuing attempts to solve these problems, many predictions of new light elementary particles and hypothetical interactions beyond the Standard Model have been made. These predictions can be constrained by many means and, specifically, by measuring the Casimir force arising between two closely spaced bodies due to the zero-point and thermal fluctuations of the electromagnetic field. After a brief survey in the theory of the Casimir effect, the strongest constraints on the power-type and Yukawa-type corrections to Newtonian gravity, following from measuring the Casimir force at short distances, are considered. Next, the problems of dark matter, dark energy and their probable constituents are discussed. This is followed by an analysis of constraints on the dark matter particles, and, specifically, on axions and axionlike particles, obtained from

---

Galina L. Klimchitskaya  
Central Astronomical Observatory at Pulkovo of the Russian Academy of Sciences, Saint Petersburg, 196140, Russia; Peter the Great Saint Petersburg Polytechnic University, Saint Petersburg, 195251, Russia, e-mail: g.klimchitskaya@gmail.com

Vladimir M. Mostepanenko  
Central Astronomical Observatory at Pulkovo of the Russian Academy of Sciences, Saint Petersburg, 196140, Russia; Peter the Great Saint Petersburg Polytechnic University, Saint Petersburg, 195251, Russia; Kazan Federal University, Kazan, 420008, Russia, e-mail: vmostepa@gmail.com

the Casimir effect. The question of whether the Casimir effect can be used for constraining the spin-dependent interactions is also considered. Then the constraints on the dark energy particles, like chameleons and symmetrons, are examined. In all cases the subject of our treatment is not only measurements of the Casimir force but some other relevant table-top experiments as well. In conclusion, the prospects of the Casimir effect for constraining theoretical predictions beyond the Standard Model at short distances are summarized.

### 13.1 Introduction: Gravity, the Standard Model and Beyond

The gravitational force is familiar to everybody from the day-to-day experience. If some body is released, it falls to earth under the influence of gravitational attraction. The laws of free fall were experimentally discovered by Galileo Galilei who found that in a vacuum the bodies of different weight fall with a uniform acceleration and reach the earth concurrently. This great (and somewhat counterintuitive) result was later derived theoretically by Newton from his second law and law of gravity under a fundamental assumption that the inertial and gravitational masses are equal (the equivalence principle).

It is common knowledge that according to Newton's law of gravity two point masses  $m_1$  and  $m_2$  separated by a distance  $r$  attract each other with the force

$$F_{gr}(r) = -\frac{dV_{gr}(r)}{dr} = -G\frac{m_1m_2}{r^2}, \quad (13.1)$$

where  $G$  is the gravitational constant and  $V_{gr}$  is the gravitational interaction energy

$$V_{gr}(r) = -G\frac{m_1m_2}{r}. \quad (13.2)$$

Einstein's general relativity theory [1] changed seriously the conceptual pattern of gravity. According to this theory, gravity is a curved space-time whose geometrical properties are determined not only by the masses of material bodies but by all components of their stress-energy tensor. It is important, however, that corrections to (13.1) and (13.2) predicted by the general relativity theory for mass and separation scales characteristic of a physical laboratory are negligibly small [2]. The gravitational force ensures the stability of planets, solar system, galaxies, and determines the structure and evolution of the whole Universe.

Another force which manifests itself in day-to-day life is the electromagnetic one. The classical theory of this force was created by Maxwell and is known as classical electrodynamics [3]. Unlike the gravitational force which is universal and acts between all material bodies, the electromagnetic force acts only between bodies possessing electric charges. The Maxwell theory describes only the classical aspects of electromagnetic interaction, whereas the full picture is given by quantum electrodynamics [4] created in the middle of the last century by Feynman, Schwinger,

Tomonaga, and Dyson. Electromagnetic forces bind nuclei and electrons into atoms, create chemical bonds which make possible the existence of molecules. They are responsible for the structure of crystal lattices and are heavily used in electronics and all modern technologies.

Two other types of fundamental forces existing in nature, weak and strong interaction, are entirely quantum. They are not visible to the naked eye. The weak interaction is responsible for a decay of many elementary particles whereas the strong interaction binds protons and neutrons into atomic nuclei. In the middle of sixties of the last century, Weinberg, Salam and Glashow developed the unified theory of weak and electromagnetic interactions [5]. For electromagnetic interaction, the intermediate particles between electrically charged particles (the so-called force carriers) are the massless photons. Photons are the specific case of gauge bosons, i.e., particles of spin one which mediate different interactions. The force carriers for a weak interaction between particles are the three massive bosons, two of which,  $W^+$  and  $W^-$ , are electrically charged and one,  $Z_0$ , is neutral.

By the middle of seventies, owing to works by Nambu, Gross, Wilczek, Politzer and other scientists, the theory of strong interactions had been elaborated. According to this theory, strongly interacting particles, e.g., protons and neutrons, consist of quarks possessing spin  $1/2$  and the new type of charge called color. Unlike the electric charge, which may be either positive or negative, the color charge has three different values (and respective anticolors). The force carriers for a strong interaction between quarks are eight massless gauge bosons called gluons which bear the color charges. Due to this the theory of strong interactions was called quantum chromodynamics [6].

The Standard Model is a unified theory of the three fundamental interactions – electromagnetic, weak, and strong [7]. According to the Standard Model, there are three pairs (generations) of quarks possessing the color charge and three pairs of spin  $1/2$  particles called leptons (the most familiar of them are electrons and respective electronic neutrinos). There are also as many antiquarks and antileptons as quarks and leptons. Next, the Standard Model includes the force carriers of electromagnetic, weak and strong interactions, i.e., photons, three massive bosons,  $W^+$ ,  $W^-$ ,  $Z^0$ , and eight gluons. Finally, an important element of the Standard Model is the heavy particle of zero spin called the Higgs boson predicted by Higgs in 1964, which is responsible for a generation of masses of other elementary particles. By now all the above elements of the Standard Model were observed in the accelerator experiments and many other theoretical predictions made on this basis found their experimental confirmation.

Great successes of the Standard Model in particle physics do not mean, however, that we already have the theory of everything. The major problem is that the general relativity theory remains to be isolated from the Standard Model, and the gravitational force avoids unification with other three fundamental interactions in spite of persistent efforts undertaken during several decades. Both Newtonian gravity and Einstein's general relativity are the entirely classical theories. However, for a description of physical phenomena happening in the close proximity of space-time singularities predicted by the general relativity theory, one evidently needs some theory which takes into account the quantum effects. There are also unresolved

problems of dark matter and dark energy which are observed only indirectly through their gravitational interactions but are not explained in the context of the Standard Model. It should be mentioned also that at short distances below a micrometer the Newton law (13.1) lacks of experimental confirmation and leaves a room for modifications at the cost of different quantum effects.

There are also other serious problems of the Standard Model. Among them one should mention the hierarchy problem, i.e., an unanswered question of why there is a difference by the factor of  $10^{24}$  between the strength of weak and gravitational interactions, the problem of neutrino mass, which was zero in the original formulation of the model but turns out to be nonzero according to precise measurements, and the problem of an asymmetry between matter and antimatter. An important problem is also the strong CP violation (i.e., the violation of invariance relative to the charge conjugation accompanied by the parity transformation) which is admitted by the formalism of quantum chromodynamics but is not observed in experiments involving only the strong interaction.

All these problems are widely discussed in the literature, and many theoretical approaches to their resolution are proposed in the framework of extended standard model, supersymmetry, supergravity [8], and string theory [9] (see also the discussions in part ?? of this book). The mentioned approaches go beyond the Standard Model and introduce additional particles, interactions, and symmetries leading to some theoretical predictions which can be verified experimentally using the powerful high energy accelerators, astrophysical observations, and laboratory experiments.

Below we consider some of these predictions which can be verified in experiments on measuring the Casimir force arising between two closely spaced uncharged material bodies due to the zero-point and thermal fluctuations of the electromagnetic field. As it is shown below, these relatively cheap and compact laboratory experiments can compete with huge accelerators in testing some important theoretical predictions beyond the Standard Model.

## 13.2 Electromagnetic Casimir Force and the Quantum Vacuum

In 1948, Casimir [10] considered two parallel, uncharged ideal metal planes in vacuum at zero temperature spaced at a distance  $a$  and calculated the zero-point energy of the electromagnetic field in the presence and in the absence of these planes, i.e., in free space. The case with the planes differs in that the tangential component of electric field and the normal component of magnetic induction vanish on their surfaces. Casimir considered a difference between the zero-point energies per unit area in the presence and in the absence of planes

$$E(a) = \hbar \int_0^\infty \frac{k_\perp dk_\perp}{2\pi} \left( \sum_{l=0}^\infty \omega_{k_\perp, l} - \frac{a}{\pi} \int_0^\infty dk_z \omega_k \right), \quad (13.3)$$

where  $\mathbf{k} = (k_x, k_y, k_z)$  is the wave vector,  $k_\perp = \sqrt{k_x^2 + k_y^2}$  is the magnitude of the wave vector projection on the planes, the prime on the summation sign divides the term with  $l = 0$  by 2, and the frequencies of the zero-point oscillations are given by the following expressions:

$$\omega_{k_\perp, l} = c \sqrt{k_\perp^2 + \left(\frac{\pi l}{a}\right)^2}, \quad \omega_k = c \sqrt{k_\perp^2 + k_z^2}. \quad (13.4)$$

Although both terms on the right-hand side of (13.3) are infinitely large, their difference is finite. Using the Abel-Plana formula for a difference between the sum and the integral [11], one obtains

$$E(a) = -\frac{\pi^2 \hbar c}{a^3} \int_0^\infty y dy \int_y^\infty \frac{\sqrt{t^2 - y^2}}{e^{2\pi t} - 1} dt. \quad (13.5)$$

Then, calculating the integrals in (13.5), one arrives at the famous Casimir result

$$E(a) = -\frac{\pi^2}{720} \frac{\hbar c}{a^3} \quad (13.6)$$

and at respective expression for the Casimir force per unit area of the plates

$$P(a) = -\frac{dE(a)}{da} = -\frac{\pi^2}{240} \frac{\hbar c}{a^4}, \quad (13.7)$$

i.e., the Casimir pressure. This pressure is some kind of a macroscopic quantum effect determined entirely by the zero-point oscillations of quantized electromagnetic field. Thus, for two ideal metal planes separated by a distance  $a = 1 \mu\text{m}$  we obtain from (13.7) an attractive pressure  $P(a) = -1.3 \text{ mPa}$ .

In a physical laboratory we deal not with ideal metals but with real material bodies made of metallic, dielectric or semiconductor materials. In 1955, Lifshitz [12] created the general theory describing the free energy and force arising between two thick material plates (semispaces) spaced at a separation  $a$  in thermal equilibrium with the environment at temperature  $T$ . The material properties in this theory were characterized by the dielectric permittivities  $\varepsilon^{(n)}(\omega)$  of the first and second plates ( $n = 1, 2$ ). Later the Lifshitz results were generalized for the plates possessing magnetic properties characterized by the magnetic permeabilities  $\mu^{(n)}(\omega)$  [13].

In the framework of the Lifshitz theory, the free energy of interaction caused by the zero-point and thermal fluctuations of the electromagnetic field per unit area of the plates is given by [12, 14]

$$\mathcal{F}(a, T) = \frac{k_B T}{2\pi} \sum_{l=0}^{\infty}{}' \int_0^\infty k_\perp dk_\perp \sum_\alpha \ln \left[ 1 - r_\alpha^{(1)}(i\xi_l, k_\perp) r_\alpha^{(2)}(i\xi_l, k_\perp) e^{-2a q_l} \right], \quad (13.8)$$

where  $k_B$  is the Boltzmann constant,  $\xi_l = 2\pi k_B T l / \hbar$  are the Matsubara frequencies,  $q_l = \sqrt{k_\perp^2 + \xi_l^2 / c^2}$ , and the reflection coefficients for two independent polarizations of the electromagnetic field, transverse magnetic ( $\alpha = \text{TM}$ ) and transverse electric ( $\alpha = \text{TE}$ ), are given by

$$\begin{aligned} r_{\text{TM}}^{(n)}(i\xi_l, k_\perp) &= \frac{\varepsilon^{(n)}(i\xi_l)q_l - k^{(n)}(i\xi_l, k_\perp)}{\varepsilon^{(n)}(i\xi_l)q_l + k^{(n)}(i\xi_l, k_\perp)}, \\ r_{\text{TE}}^{(n)}(i\xi_l, k_\perp) &= \frac{\mu^{(n)}(i\xi_l)q_l - k^{(n)}(i\xi_l, k_\perp)}{\mu^{(n)}(i\xi_l)q_l + k^{(n)}(i\xi_l, k_\perp)}, \end{aligned} \quad (13.9)$$

where

$$k^{(n)}(i\xi_l, k_\perp) = \sqrt{k_\perp^2 + \varepsilon^{(n)}(i\xi_l)\mu^{(n)}(i\xi_l)\frac{\xi_l^2}{c^2}}. \quad (13.10)$$

In a similar way, the Casimir force per unit area of real material plates is expressed as

$$\begin{aligned} P(a, T) &= -\frac{\partial \mathcal{F}(a, T)}{\partial a} = -\frac{k_B T}{\pi} \sum_{l=0}^{\infty} \int_0^{\infty} q_l k_\perp dk_\perp \\ &\times \sum_{\alpha} \left[ \frac{e^{2aq_l}}{r_{\alpha}^{(1)}(i\xi_l, k_\perp)r_{\alpha}^{(2)}(i\xi_l, k_\perp)} - 1 \right]^{-1}. \end{aligned} \quad (13.11)$$

Taking into account that ideal metal is the perfect reflector, so that

$$r_{\text{TM}}^{(n)}(i\xi_l, k_\perp) = -r_{\text{TE}}^{(n)}(i\xi_l, k_\perp) = 1 \quad (13.12)$$

at all  $\xi_l$ , at  $T = 0$  one obtains from (13.8) and (13.11) the Casimir results (13.6) and (13.7). In the limiting case of small separations, (13.8) and (13.11) describe the familiar van der Waals force which depends on  $\hbar$  but does not depend on the speed of light  $c$ . In the opposite limiting case of large separations, the resulting free energy and force do not depend either on  $\hbar$  or  $c$ . This is the so-called classical regime where the Casimir interaction depends only on  $T$ .

Precise measurements of the Casimir force allowing quantitative comparison between experiment and theory were performed by means of an atomic force microscope, whose sharp tip was replaced with a relatively large sphere, and a micro-mechanical torsional oscillator (see [14, 15] for a review). All these experiments measured the Casimir force not between two parallel plates but between a sphere and a plate. The Casimir force between a sphere of radius  $R$  and a plate  $F^{SP}(a, T)$  can be calculated in the framework of the Lifshitz theory using the proximity force approximation [14, 15]

$$F^{SP}(a, T) = 2\pi R \mathcal{F}(a, T), \quad (13.13)$$

where the Casimir free energy between two parallel plates  $\mathcal{F}$  is given by the Lifshitz formula (13.8). Exact calculations of the Casimir force in sphere-plate geometry

using the scattering approach [16, 17, 18, 19] and the gradient expansion [20, 21, 22, 23, 24] have shown that the errors introduced by (13.13) are less than  $a/R$ , i.e., less than a fraction of a percent in the most of experimental configurations.

By calculating the derivative of (13.13) with respect to separation, one can express another quantity measured in many experiments, i.e., the gradient of the Casimir force in sphere-plate geometry via the Casimir force (13.11) per unit area of two parallel plates

$$\frac{\partial}{\partial a} F^{SP}(a, T) = -2\pi RP(a, T). \quad (13.14)$$

For comparison of theoretical predictions with the measurement data of precise experiments, one should compute the Casimir free energy (13.8) and the Casimir pressure (13.11) with sufficient precision. To do so, one needs to have the values of dielectric permittivities of plate materials at sufficiently large number of pure imaginary Matsubara frequencies. This is usually achieved by means of the Kramers-Kronig relation using the measured optical data for the complex indices of refraction of plate materials. In doing so the terms of the Lifshitz formulas (13.8) and (13.11) with  $l = 0$  play an important role in obtaining the physically correct results.

Unfortunately, the optical data are available at only sufficiently high frequencies  $\omega \geq \omega_{\min}$ . Because of this, the obtained dielectric permittivity is usually extrapolated down to zero frequency using some theoretical model. For experiments with metallic test bodies, which are used below for testing the predictions beyond the Standard Model, the most reasonable extrapolation seems to be by means of the well tested Drude model. In this case, the dielectric permittivities of plate materials take the form

$$\varepsilon_D^{(n)}(i\xi_l) = \varepsilon_c^{(n)}(i\xi_l) + \frac{\omega_{p,n}^2}{\xi_l(\xi_l + \gamma_n)}, \quad (13.15)$$

where  $\varepsilon_c^{(n)}(i\xi_l)$  is a contribution due to core electrons determined by the optical data,  $\omega_{p,n}$  is the plasma frequency and  $\gamma_n$  is the relaxation parameter.

It turned out, however, that the measurement data of all precise experiments with nonmagnetic (Au) metals [25, 26, 27, 28, 29, 30, 31, 32, 33] and magnetic (Ni) metals [34, 35, 36, 37] exclude the theoretical predictions of the Lifshitz theory using the dielectric functions (13.15). Specifically, for two test bodies made of Ni a disagreement between experiment and theory in measurements of the differential Casimir force is up to a factor of 1000 [37]. If, however, one makes an extrapolation by means of the plasma model, i.e., puts  $\gamma_n = 0$  in (13.15),

$$\varepsilon_p^{(n)}(i\xi_l) = \varepsilon_c^{(n)}(i\xi_l) + \frac{\omega_{p,n}^2}{\xi_l^2}, \quad (13.16)$$

the predictions of the Lifshitz theory come to a very good agreement with the measurement data of all precise experiments [25, 26, 27, 28, 29, 30, 31, 32, 33, 34, 35, 36, 37].

This situations calls for some clarification because at low frequencies conduction electrons really possess relaxation properties described by the phenomenological

parameter  $\gamma_n$ . It is then unclear why one should put  $\gamma_n = 0$  in computations of the Casimir force. Although the ultimate answer to this question is not found yet, theory suggests some plausible explanation. First of all, it was proven [38, 39, 40, 41] that for metals with perfect crystal lattices the Casimir entropy calculated using the dielectric permittivity (13.15) violates the third law of thermodynamics, the Nernst heat theorem, but satisfies it if the permittivity (13.16) is used.

Next, for graphene, which is a novel 2D material [42], the dielectric permittivity is not of a model character. At low energies characteristic for the Casimir effect, the dielectric properties of graphene can be calculated on the basis of first principles of quantum electrodynamics at nonzero temperature using the polarization tensor in (2+1)-dimensional space-time [43, 44]. It was found that graphene is described by two spatially nonlocal dielectric permittivities, i.e., depending on both the frequency  $\omega$  and the 2D wave vector  $\mathbf{k}$  [45, 46]. The Lifshitz theory using these permittivities turned out to be in perfect agreement with measurements of the Casimir force from graphene [47, 48, 49, 50] and with the Nernst heat theorem [51, 52, 53, 54, 55].

This suggests that the model dielectric permittivity (13.15), which is well-checked for the propagating electromagnetic waves on the mass shell in vacuum, may be inapplicable to the evanescent (off-the-mass-shell) waves. The latter contribute essentially to the Casimir free energy and force (13.8) and (13.11) caused by the electromagnetic fluctuations. First steps on the road to justification of this conjecture were made by the recently proposed spatially nonlocal dielectric permittivities which describe nearly the same response, as does the Drude model, to the propagating waves but an alternative response to the evanescent ones [56, 57]. The Lifshitz theory employing these permittivities is in as good agreement with measurements of the Casimir force between nonmagnetic metals and with the Nernst heat theorem as when it uses the plasma model (13.16) [56, 57, 58]. Recently it was also shown that it agrees equally well with measurements of the Casimir force between magnetic metals [57, 59].

By and large one can conclude that although there is a continuing discussion in the literature on theoretical description of the Casimir interaction between real material bodies (see [60] for a review), the predictions of the Lifshitz theory are now found in good agreement with the measurement data of all precise experiments and the measure of this agreement can be used for constraining the hypothetical forces of nonelectromagnetic origin.

### 13.3 Testing the Power-Type Corrections to Newtonian Gravity from the Casimir Effect

From the point of view of quantum field theory, the gravitational interaction energy (13.2) can be considered as originating from an exchange of one massless particle between two massive particles  $m_1$  and  $m_2$ . Exactly in this way the Coulomb potential is derived in quantum electrodynamics by considering an exchange of one photon between two charged particles.



The Standard Model does not contain massless particles in a free state except of photons (gluons are confined inside of barions). There are, however, massless particles predicted by some extensions of the Standard Model. For instance, theory of electroweak interactions with an extended Higgs sector predicts pseudoscalar massless particles called arions [61]. An exchange of one arion between electrons belonging to atoms of two neighboring test bodies leads to the spin-dependent effective potential which averages to zero when integrating over their volumes. The spin-independent effective potential decreasing with separation as  $r^{-3}$  arises from the process of two-arions exchange [62].

In a similar way, the effective potential decreasing with separation as  $r^{-5}$  arises from an exchange of neutrino-antineutrino pair between two neutrons [63, 64]. The power-type potentials result also from an exchange of even numbers of goldstinos which are the massless fermions introduced in the theoretical schemes with a spontaneously broken supersymmetry [65] and other predicted particles.

Taking into account that the power-type interactions with different powers coexist with the gravitational potential, the resulting interaction energy is usually represented as

$$V_l(r) = -\frac{Gm_1m_2}{r} \left[ 1 + \Lambda_l \left( \frac{r_0}{r} \right)^{l-1} \right], \quad (13.17)$$

where  $\Lambda_l$  is the dimensionless interaction constant,  $l = 1, 2, 3, \dots$ , and  $r_0$  with the dimension of length is introduced to preserve the dimension of energy for  $V_l(r)$ . Following many authors, we put  $r_0 = 1 \text{ F} = 10^{-15} \text{ m}$ . For  $l = 1$ , the quantity  $1 + \Lambda_1$  has the meaning of a factor connecting the values of inertial and gravitational masses, for  $l = 3$  the second term in (13.17) presents a correction to the Newtonian potential due to an exchange of two arions, and for  $l = 5$  — due to an exchange of neutrino-antineutrino pair.

The power-type corrections to Newton's law arise not only due to an exchange of massless hypothetical particles but in extensions of the Standard Model which exploit the extra-dimensional unification schemes with noncompact but warped extra dimensions. In this case, the modified gravitational interaction energy at separations  $r \gg K_w$  takes the form [66, 67]

$$V_3(r) = -\frac{Gm_1m_2}{r} \left( 1 + \frac{2}{3K_w^2 r^2} \right), \quad (13.18)$$

where  $K_w$  is the warping scale. This is the potential of the form of (13.17) with  $\Lambda_3 = 2/(3K_w^2 r_0^2)$ .

Constraints on the values of interaction constant  $\Lambda_l$  with different  $l$  can be obtained from the gravitational experiments of Eötvos and Cavendish type. In the Eötvos-type experiments one verifies a validity of the equivalence principle, i.e., places limits on possible deviations between the inertial and gravitational masses. Using (13.17), these limits can be recalculated in the constraints on  $\Lambda_1$ . Thus, from the most precise short-range Eötvos-type experiments [68, 69] the constraint  $|\Lambda_1| \leq 1 \times 10^{-9}$  was obtained.

In the Cavendish-type experiments, one measures probable deviations of the force acting between two bodies from the Newton law (13.1). From the power-type interaction energy (13.17) one finds the respective force

$$F_l(r) = -\frac{dV_l(r)}{dr} = -\frac{Gm_1m_2}{r^2} \left[ 1 + l\Lambda_l \left( \frac{r_0}{r} \right)^{l-1} \right]. \quad (13.19)$$

Then the constraints on  $\Lambda_l$  can be found from the measured limits on the dimensionless quantity

$$\varepsilon_l = \frac{1}{rF_l(r)} \frac{d}{dr} [r^2 F_l(r)], \quad (13.20)$$

which is equal to zero if  $\Lambda_l = 0$ , i.e., no power-type interaction in addition to gravity is present. Using this approach, from the Cavendish-type experiment [70] the following constraints on  $\Lambda_l$  were obtained [71]:  $|\Lambda_2| \leq 4.5 \times 10^8$ ,  $|\Lambda_3| \leq 1.3 \times 10^{20}$ ,  $|\Lambda_4| \leq 4.9 \times 10^{31}$ ,  $|\Lambda_5| \leq 1.5 \times 10^{43}$ .

In [62, 72] it was suggested to obtain constraints on the power-type interactions from measurements of the Casimir force. The Casimir force  $F^{LP}(a)$  between a spherical lens of centimeter-size radius and a plate both made of quartz was measured at distances  $a \leq 1 \mu\text{m}$  in [73] with a relative error  $\Delta F/F^{LP} \approx 10\%$ , where  $\Delta F$  is the absolute error. In the limits of this error, the measurement data were found to be in agreement with theoretical predictions of the Lifshitz theory.

Any hypothetical interaction energy of power type between an atom of the lens at a point  $\mathbf{r}_1$  and an atom of the plate at a point  $\mathbf{r}_2$  is given by (13.17) where  $r = |\mathbf{r}_1 - \mathbf{r}_2|$ . Then, the total interaction force between the experimental test bodies (the lens and the plate) is given by the integration over their volumes  $V_1$  and  $V_2$  with subsequent negative differentiation with respect to the distance  $a$  of their closest approach

$$F_l^{LP}(a) = -n_1 n_2 \frac{\partial}{\partial a} \int_{V_1} d^3 r_1 \int_{V_2} d^3 r_2 V_l(|\mathbf{r}_1 - \mathbf{r}_2|), \quad (13.21)$$

where  $n_1$  and  $n_2$  are the numbers of atoms per unit volume of the first and second test bodies. In doing so, one can neglect by the Newtonian contribution on the right-hand side of (13.21) because it is negligibly small as compared to the experimental error in the micrometer separation range.

Taking into account that no additional interaction was observed within the limits of measurement errors, the constraints on  $\Lambda_l$  with  $l = 1, 2, 3, 4$ , and  $5$  were obtained from the inequality [62, 72]

$$|F_l^{LP}(a)| \leq \Delta F(a). \quad (13.22)$$

Among these constraints, that ones on  $\Lambda_2$  and  $\Lambda_3$  turned out to be stronger as compared with constraints found from older Cavendish-type experiments available in 1987 [74].

It would be interesting to estimate potentialities of modern measurements of the Casimir force for constraining the power-type interactions. For this purpose we consider the most recent experiment [33] on measuring the Casimir force between an

Au-coated sphere of  $R = 149.7 \mu\text{m}$  radius and an Au-coated plate in the micrometer separation range. The sphere is spaced at a height  $a$  above the plate. To estimate the strongest constraints that could be obtained from the experiments of this kind, we consider both the sphere and the plate as all-gold (in real experiment the sapphire sphere and silicon plate were coated with Au films of 250 and 150 nm thicknesses, respectively). The plate can be considered as infinitely large because its size was much larger than the sphere radius.

Let the plate top be in the plane  $z = 0$  and an atom of the sphere has the coordinates  $\mathbf{r}_1 = (0, 0, z)$ . For all powers  $l \geq 3$  in (13.17) the plate can be considered as infinitely thick. The atom-plate force arising due to the second contribution on the right-hand side of (13.17) is given by

$$\begin{aligned} F_l^{AP}(a) &= Gm_1m_2n_2\Lambda_l r_0^{l-1} \frac{\partial}{\partial z} \int_{V_2} d^3r_2 \frac{1}{|\mathbf{r}_1 - \mathbf{r}_2|^{l-1}} \\ &= -\frac{2\pi}{l-2} G\rho_2m_1\Lambda_l r_0^{l-1} \frac{1}{z^{l-2}}, \end{aligned} \quad (13.23)$$

where  $\rho_2 = m_2n_2$  is the mass density of the plate material (Au).

Now we integrate (13.23) over the volume of a sphere. The density of atoms at a height  $z \geq a$  in thin horizontal layer of the sphere is given by

$$\pi n_1 [2R(z-a) - (z-a)^2]. \quad (13.24)$$

Then, the sphere-plate force is found by integrating (13.23) with the weight (13.24)

$$F_l^{SP}(a) = -\frac{2\pi^2}{l-2} G\rho_1\rho_2\Lambda_l r_0^{l-1} \int_a^{2R+a} \frac{2R(z-a) - (z-a)^2}{z^{l-2}} dz, \quad (13.25)$$

where  $\rho_1 = m_1n_1$  is the mass density of the sphere material (in our case also Au).

Introducing the new integration variable  $t = z - a$ , we rewrite (13.25) in the form

$$F_l^{SP}(a) = -\frac{2\pi^2}{l-2} G\rho_1\rho_2\Lambda_l r_0^{l-1} \int_0^{2R} \frac{2Rt - t^2}{(a+t)^{l-2}} dt. \quad (13.26)$$

Finally, calculating the integral in (13.26), one arrives at

$$F_l^{SP}(a) = -\frac{2\pi^2}{l-2} G\Lambda_l\rho_1\rho_2 \frac{r_0^{l-1}R^3}{a^{l-2}} {}_2F_1(l-2, 2; 3; -2Ra^{-1}), \quad (13.27)$$

where  ${}_2F_1(a, b; c; z)$  is the hypergeometric function.

Substituting (13.27) in place of  $F_l^{LP}$  in (13.22), one finds the strongest constraints on  $\Lambda_l$  obtainable from the experiment [33] if it would be performed with the all-gold test bodies. The numerical analysis shows that the most strong constraints follow at  $a = 3 \mu\text{m}$  where  $\Delta F(a) = 2.2 \text{ fN}$  [33]. The obtained constraints are:  $|\Lambda_3| \leq 1.3 \times 10^{23}$ ,  $|\Lambda_4| \leq 1.8 \times 10^{34}$ , and  $|\Lambda_5| \leq 5.6 \times 10^{44}$ . It is seen that these

constraints are weaker than those mentioned above following from the Cavendish-type experiment [70, 71].

The case of  $l = 2$  should be considered separately. In this case, it is necessary to take into account the finite thickness of the plate  $D = 50 \mu\text{m}$  because for  $l = 2$  an integral over the plate of infinitely large thickness (i.e., over the semispace) diverges. By performing calculations in the same way as above, one obtains

$$F_2^{SP}(a) = -\frac{2\pi^2}{3} \rho_1 \rho_2 G \Lambda_2 r_0 \left[ 2RD(2a + 2R + D) + (a + 3R)a^2 \ln \frac{a + 2R}{a} - (a + D)^2(a + 3R + D) \ln \frac{a + 2R + D}{a + D} + 4R^3 \ln \frac{a + 2R + D}{a + 2R} \right]. \quad (13.28)$$

Substituting (13.28) in (13.22) in place of  $F_l^{LP}$  and using  $\Delta F(a) = 2.2 \text{ fN}$ , one finds  $|\Lambda_2| \leq 2.85 \times 10^{12}$ . This is again a much weaker constraint than that obtained in [71] based on the Cavendish-type experiment [70]. One can conclude that the short-separation Cavendish-type experiments are more prospective for constraining the power-type hypothetical interactions than measurements of the Casimir force.

This conclusion finds further confirmation from the recently performed Cavendish-type experiment which presents an improved test of Newton's gravitational law at short separations [75]. The constraints on  $\Lambda_l$  with  $l = 2, 3, 4$ , and 5 obtained in this work are somewhat stronger than those cited above [70, 71]. In Table 13.1 (line 1) we present the strongest constraint on  $\Lambda_1$  following from the Eötvos-type experiment [68]. In columns 2 and 3 (lines 2–5), the strongest constraints  $\Lambda_l$  with  $l = 2, 3, 4$ , and 5 following from the Cavendish-type experiments [71] and [75], respectively, are presented. As is seen in Table 13.1, the strength of constraints quickly drops with increase of the interaction power.

**Table 13.1** The strongest constraints on the constants of power-type hypothetical interaction following from the Eötvos-type (line 1) and Cavendish-type (lines 2–5) experiments.

1	$ \Lambda_l _{\max}$		$ \Lambda_l _{\max}$	
1	$1 \times 10^{-9}$	[68]	$1 \times 10^{-9}$	[68]
2	$4.5 \times 10^8$	[71]	$3.7 \times 10^8$	[75]
3	$1.3 \times 10^{20}$	[71]	$7.5 \times 10^{19}$	[75]
4	$4.9 \times 10^{31}$	[71]	$2.2 \times 10^{31}$	[75]
5	$1.5 \times 10^{43}$	[71]	$6.7 \times 10^{42}$	[75]

### 13.4 Testing the Yukawa-Type Corrections to Newtonian Gravity from the Casimir Effect

The interaction energy of Yukawa type between two pointlike particles (atoms or molecules) separated by a distance  $r$  arises due to an exchange of one light scalar

particle. The Standard Model considered in Sect. 13.1 contains only one scalar particle, the Higgs boson, which is very heavy and cannot serve as an exchange boson in long-range interactions. The extensions of the Standard Model predict, however, a number of light scalar particles such as moduli [76], which arise in supersymmetric theories, dilaton [77], which appears in extra-dimensional models with the varying volume of compactified dimensions, scalar axion [78], which is a superpartner of an axion, etc. (see Sect. 13.5 and also the discussions on scalar-teleparallel and scalar-tensor theories in Chapters ??, ?? and ??).

Similar to the power-type interactions, the interaction of Yukawa type between two particles of masses  $m_1$  and  $m_2$  coexists with gravity and is usually parametrized as

$$V_{\text{Yu}}(r) = -\frac{Gm_1m_2}{r} \left(1 + \alpha e^{-r/\lambda}\right), \quad (13.29)$$

where  $\alpha$  is the dimensionless interaction constant and  $\lambda$  is the interaction range having the meaning of the Compton wavelength of exchange scalar particle of mass  $m_s$ :  $\lambda = \hbar/(m_s c)$ .

Another prediction of the Yukawa-type correction to Newton's gravitational law comes from the extra-dimensional models with compact extra dimensions and low-energy compactification scale [79, 80]. In the framework of this approach beyond the Standard Model, the space-time has  $D = 4 + N$  dimensions where  $N$  extra dimensions are compactified at relatively low Planck energy scale in  $D$  dimensions

$$E_{\text{Pl}}^{(D)} = \left(\frac{\hbar^{1+N} c^{5+N}}{G_D}\right)^{\frac{1}{2+N}} \sim 1 \text{ TeV}. \quad (13.30)$$

Here,  $G_D$  is the gravitational constant in the extended  $D$ -dimensional space-time  $G_D = G\Omega_N$  and  $\Omega_N \sim R_*^N$ ,  $R_*$  being the size of compact manifold.

In fact the approach under consideration was suggested as a possible solution of hierarchy problem discussed in Sect. 13.1 since due to (13.30) the characteristic energy scales of the gravitational and gauge interactions of the Standard Model coincide. In doing so the size of compact manifold is given by [80]

$$R_* \sim \frac{\hbar c}{E_{\text{Pl}}^{(D)}} \left[ \frac{E_{\text{Pl}}}{E_{\text{Pl}}^{(D)}} \right]^{\frac{2}{N}} \sim 10^{\frac{32-17N}{N}}, \quad (13.31)$$

where the usual Planck energy  $E_{\text{Pl}} = (\hbar c^5/G)^{1/2} \sim 10^{19}$  GeV.

According to the developed approach, the standard Newton law (13.1) and (13.2) is not valid in  $D$ -dimensional space-time. It was shown [81, 82] that at separations  $r \gg R_*$  the gravitational interaction energy takes the form (13.29) with  $\lambda \sim R_*$ . Although for one extra dimension ( $N = 1$ ) equation (13.31) leads to too large  $R_* \sim 10^{15}$  cm, which is excluded by the tests of Newton's law in the solar system [83], for  $N = 2$  and 3 (13.31) leads to the more realistic results  $R_* \sim 1$  mm and  $R_* \sim 5$  nm, respectively. This means that a search for deviations from the Newton

law at short distances is not only a quest for hypothetical particles, but for extra dimensions as well.

Constraints on the parameters of Yukawa-type interaction  $\alpha$  and  $\lambda$  can be obtained from the Cavendish-type experiments. The potential energy (13.29) results in the force acting between two particles  $m_1$  and  $m_2$

$$F_{\text{Yu}}(r) = -\frac{dV_{\text{Yu}}(r)}{dr} = -\frac{Gm_1m_2}{r^2} \left[ 1 + \alpha e^{-r/\lambda} \left( 1 + \frac{r}{\lambda} \right) \right]. \quad (13.32)$$

Then the quantity

$$\varepsilon_{\text{Yu}} = \frac{1}{rF_{\text{Yu}}(r)} \frac{d}{dr} [r^2 F_{\text{Yu}}(r)] \quad (13.33)$$

is not equal to zero due to a nonzero strength of the Yukawa force  $\alpha$ . The deviation of this quantity from zero (if any) could be determined from the results of Cavendish-type experiments. Depending on the range of  $\lambda$ , different Cavendish-type experiments lead to the strongest constraints on  $\alpha$ . For  $8 \mu\text{m} < \lambda < 9 \mu\text{m}$  the most strong constraints follow from the short-range test of Newtonian gravity at 20 micrometers [84]. The Cavendish-type experiment [70], already discussed in Sect. 13.3 in the context of power-type interactions, leads to the strongest constraints on  $\alpha$  within the wide interaction range  $9 \mu\text{m} < \lambda < 4 \text{mm}$  [71]. It should be noted, however, that in the part of this interval  $40 \mu\text{m} < \lambda < 0.35 \text{mm}$  the obtained results have been strengthened by up to a factor of 3 in the refined experiment [75] which was also mentioned in Sect. 13.3. Finally, an older Cavendish-type experiment [85] performed at larger separations allows obtaining the strongest constraints on  $\alpha$  in the range  $4 \text{mm} < \lambda < 1 \text{cm}$ . In the range of even larger  $\lambda$ , unrelated to the Casimir force, the strongest constraints on  $\alpha$  follow from the Eötvos-type experiments [69, 86].

In Fig. 13.1, we present the constraints on  $\alpha$  obtained from different gravitational experiments by the line labeled gr. Only the range of  $\lambda$  below  $66 \mu\text{m}$  is included neighboring to the region considered below where the strongest constraints on  $\alpha$  follow from experiments performed in the Casimir regime. The values of parameters of the Yukawa-type interaction belonging to the area of  $(\lambda, \alpha)$  plane above the line are excluded by the results of Cavendish-type experiments mentioned above, whereas the area of the same plane below the line is allowed. At  $\lambda = 8 \mu\text{m}$  the line gr intersects with the end of the line Casimir-less which is discussed below in this section.

As is seen in Fig. 13.1, the strength of constraints obtained from gravitational experiments quickly drops with decreasing  $\lambda$ . As an example, for  $r = \lambda = 10 \mu\text{m}$  the Cavendish-type experiments do not exclude an existence of the Yukawa-type force between two particles which exceeds the Newtonian gravitational force by the factor of  $10^4$ . This means that the Newtonian law of gravitation lacks of sufficient experimental confirmation at short separations which prevents obtaining strong constraints on some other forces from gravitational experiments.

In fact at separations of the order of micrometer and less the main background force between two material bodies far exceeding the gravitational interaction is the Casimir force considered in Sect. 13.2. In [87] it was suggested to constrain the

hypothetical Yukawa-type interaction from experiments on measuring the van der Waals and Casimir forces.

Similar to the case of power-type interactions, the Yukawa-type force acting between two test bodies spaced at a closest separation  $a$  can be obtained by an integration of the interaction energy (13.29) over their volumes with subsequent negative differentiation with respect to  $a$

$$F_{\text{Yu}}^{V_1 V_2}(a) = -n_1 n_2 \frac{\partial}{\partial a} \int_{V_1} d^3 r_1 \int_{V_2} d^3 r_2 V_{\text{Yu}}(|\mathbf{r}_1 - \mathbf{r}_2|). \quad (13.34)$$

Taking into account that within the experimental error  $\Delta F(a)$  the measured Casimir force was found to be in agreement with theoretical predictions, the constraints on  $F_{\text{Yu}}$  can be found from the inequality

$$|F_{\text{Yu}}^{V_1 V_2}(a)| \leq \Delta F(a). \quad (13.35)$$

Following this approach, the first constraints on the Yukawa-type interaction with  $\lambda < 20$  cm were obtained [87] from two experiments [73, 88] performed long ago.

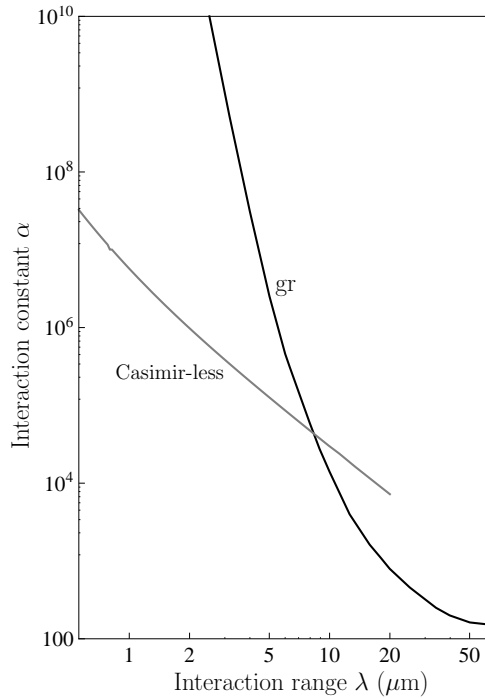


**Fig. 13.1** Constraints on the interaction constant  $\alpha$  of Yukawa-type interaction are shown as functions of the interaction range  $\lambda$  by the lines labeled gr and Casimir-less obtained from the gravitational and Casimir-less experiments, respectively. The regions of  $(\lambda, \alpha)$  plane above each line are excluded and below are allowed

During the last twenty years many experiments on measuring the Casimir interaction have been performed (some of them are mentioned in Sect. 13.2). All these experiments use the configuration of a sphere above a plate which surfaces may be coated by some additional material layers or covered with sinusoidal corrugations. We start with the simplest configuration of a smooth sphere of radius  $R$  at the closest separation  $a$  above a large smooth plate of thickness  $D$ . We again consider an atom  $m_1$  of the sphere at a height  $z$  above the plate and integrate the Yukawa interaction energy (13.29) over the plate volume  $V_2$  with subsequent negative differentiation according to (13.34). As explained above, the contribution of gravitational interaction can be neglected. Then, similar to (13.23), for the atom-plate force one obtains

$$F_{\text{Yu}}^{AP}(z) = -2\pi G\rho_2 m_1 \alpha \lambda e^{-z/\lambda} \left(1 - e^{-D/\lambda}\right). \quad (13.36)$$

Now we integrate (13.36) over the sphere volume using (13.24) and obtain the Yukawa-type force acting between a sphere and a plate [89]

$$\begin{aligned} F_{\text{Yu}}^{AP}(a) &= -2\pi^2 G\rho_1 \rho_2 \alpha \lambda \left(1 - e^{-D/\lambda}\right) \int_a^{2R+a} dz [2R(z-a) - (z-a)^2] e^{-z/\lambda} \\ &= -4\pi^2 G\rho_1 \rho_2 \alpha \lambda^3 \left(1 - e^{-D/\lambda}\right) e^{-a/\lambda} \Phi(R, \lambda), \end{aligned} \quad (13.37)$$

where the following notation is introduced

$$\Phi(r, \lambda) = r - \lambda + (r + \lambda)e^{-2r/\lambda}. \quad (13.38)$$

The strongest current constraints on the Yukawa-type force in the wide interaction range from 10 nm to 8  $\mu\text{m}$  follow from four experiments of the Casimir physics.

The first of them is devoted to measurements of the lateral Casimir force between the surfaces of a sphere and a plate covered with coaxial longitudinal sinusoidal corrugations and coated with an Au film [90, 91]. This experiment was performed by means of an atomic force microscope.

The respective constraints were obtained in [92]. For this purpose, the interaction energy of Yukawa type between the corrugated test bodies was calculated by integrating (13.29) over their volumes, and the lateral force was found by the negative differentiation of the obtained result with respect to the phase shift between corrugations (see [92] for details). The obtained constraints cover a wide interaction range but currently they are the strongest ones only in the narrow region  $10 \text{ nm} < \lambda < 11.6 \text{ nm}$  (see the line labeled 1 in Fig. 13.2).

The second experiment, also performed by using an atomic force microscope, is on measuring the usual (normal) Casimir force between the sinusoidally corrugated Au-coated surfaces of a sphere and a plate under some angle between the corrugation axes [93, 94]. The constraints on the Yukawa parameters  $\alpha$  and  $\lambda$ , following from this experiment, were obtained in [95]. Currently, these constraints remain the strongest ones in the region  $11.6 \text{ nm} < \lambda < 17.2 \text{ nm}$ . They are shown by the line labeled 2 in Fig. 13.2.



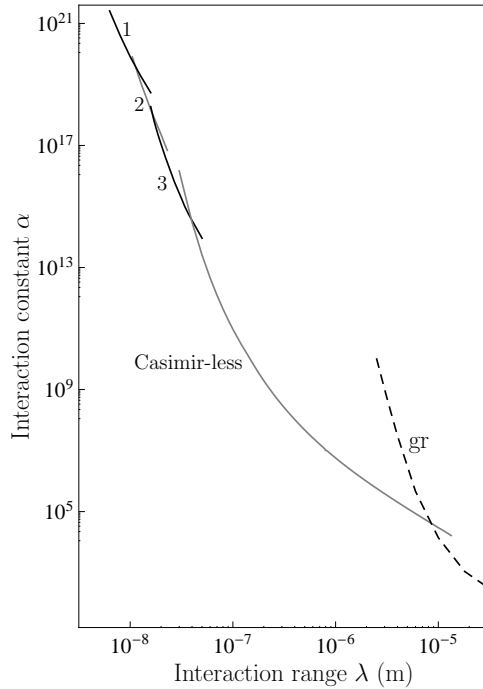


**Fig. 13.2** Constraints on the interaction constant  $\alpha$  of Yukawa-type interaction are shown as functions of the interaction range  $\lambda$  by the lines labeled 1, 2, 3, Casimir-less, and gr obtained from measuring the lateral and normal Casimir forces between the sinusoidally corrugated surfaces, effective Casimir pressure, from the Casimir-less experiment, and gravitational experiments, respectively. The regions of  $(\lambda, \alpha)$  plane above each line are excluded and below are allowed

In the next, third, experiment the effective Casimir force per unit area of two Au-coated plates (i.e., the effective Casimir pressure) was determined by means of a micromechanical torsional oscillator [27, 28]. In fact it was recalculated from the directly measured gradient of the Casimir force,  $F'_{sp}$ , between a sphere and a plate using (13.14). In the same way, calculating the gradient of (13.37) one finds from (13.14) the Yukawa-type pressure between two parallel plates

$$P_{Yu}(a) = -2\pi G\rho_1\rho_2\alpha\lambda^2 \left(1 - e^{-D/\lambda}\right) e^{-a/\lambda}. \quad (13.39)$$

Here, following [27, 28], we took into account that  $\lambda \ll R$  leading to  $\Phi(R, \lambda) \approx R$ .

In this experiment, the test bodies were not homogeneous. A sapphire sphere of density  $\rho_s = 4.1 \text{ g/cm}^3$  was coated with the first layer of Cr with density  $\rho_{Cr} = 7.14 \text{ g/cm}^3$  and thickness  $\Delta_1 = 10 \text{ nm}$ , and then with the second, external, layer of Au of density  $\rho_{Au} = 19.28 \text{ g/cm}^3$  and thickness  $\Delta_2 = 180 \text{ nm}$ . The plate was made of Si with density  $\rho_{Si} = 2.33 \text{ g/cm}^3$  and coated with a layer of Cr of thickness  $\Delta_1 = 10 \text{ nm}$  and external layer of Au of thickness  $\Delta_2 = 210 \text{ nm}$ . Taking into account that the layers contribute to the Casimir pressure additively, we obtain from (13.39) the following expression valid in the experimental configuration

$$P_{\text{Yu}}(a) = -2\pi G\alpha\lambda^2 e^{-a/\lambda} \left[ \rho_{\text{Au}} - (\rho_{\text{Au}} - \rho_{\text{Cr}})e^{-\Delta_2/\lambda} - (\rho_{\text{Cr}} - \rho_s)e^{-(\Delta_2+\Delta_1)/\lambda} \right] \\ \times \left[ \rho_{\text{Au}} - (\rho_{\text{Au}} - \rho_{\text{Cr}})e^{-\tilde{\Delta}_2/\lambda} - (\rho_{\text{Cr}} - \rho_{\text{Si}})e^{-(\tilde{\Delta}_2+\Delta_1)/\lambda} \right]. \quad (13.40)$$

The constraints on the Yukawa parameters  $\alpha$  and  $\lambda$  were obtained from the inequality

$$|P_{\text{Yu}}(a)| \leq \Delta P(a), \quad (13.41)$$

where the experimental error  $\Delta P(a)$  in measuring the effective Casimir pressure, with which the theoretical predictions of the Lifshitz theory were confirmed, was determined at the 95% confidence level. Currently, the constraints obtained from this experiment are the strongest ones over the interaction range  $17.2 \text{ nm} < \lambda < 39 \text{ nm}$ . They are found from (13.41) at  $a = 180 \text{ nm}$  where  $\Delta P(a) = 4.8 \text{ mPa}$  [27, 28] and shown by the line labeled 3 in Fig. 13.2.

The last, fourth, experiment leading to the strongest constraints on the Yukawa-type interaction over a wide interaction range  $39 \text{ nm} < \lambda < 8 \text{ }\mu\text{m}$  is performed in such a way, that the contribution of the Casimir force to the measured signal is nullified [96]. This was achieved by measuring the differential force between a sphere of  $R = 149.3 \text{ }\mu\text{m}$  radius and an especially structured plate using a micromechanical torsional oscillator. The sphere made of sapphire was coated with a  $\Delta_1 = 10 \text{ nm}$  layer of Cr and  $\Delta_2 = 250 \text{ nm}$  layer of Au. The plate consisted of Si and Au parts of  $D = 2.1 \text{ }\mu\text{m}$  thickness both coated with a Cr and Au overlayers of thicknesses  $\Delta_1 = 10 \text{ nm}$  and  $\tilde{\Delta}_2 = 150 \text{ nm}$ , respectively.

The Casimir forces between a sphere and two halves of the patterned Au-Si plate are equal because the thickness of an Au overlayer is sufficiently large in order it could be considered as a semispace [14]. As a result, when the sphere is moved back and forth above the patterned plate, the measured differential force is equal to a difference of the Yukawa-type forces between a sphere and two halves of the plate. Using (13.37) with  $\Phi(R, \lambda) \approx R$  and taking into account the Au and Cr layers covering the test bodies, the differential Yukawa-type force takes the form

$$F_{\text{Yu,Au}}^{SP}(a) - F_{\text{Yu,Si}}^{SP}(a) = -4\pi^2 G\alpha\lambda^3 R (\rho_{\text{Au}} - \rho_{\text{Si}}) e^{-(a+\tilde{\Delta}_2+\Delta_1)/\lambda} \left( 1 - e^{-D/\lambda} \right) \\ \times \left[ \rho_{\text{Au}} - (\rho_{\text{Au}} - \rho_{\text{Cr}})e^{-\Delta_2/\lambda} - (\rho_{\text{Cr}} - \rho_s)e^{-(\Delta_2+\Delta_1)/\lambda} \right]. \quad (13.42)$$

The constraints have been obtained from the inequality

$$|F_{\text{Yu,Au}}^{SP}(a) - F_{\text{Yu,Si}}^{SP}(a)| \leq \Xi(a), \quad (13.43)$$

where a sensitivity of the setup to force differences  $\Xi(a)$  is equal to a fraction of 1 fN. Note that both the residual electric and Newtonian gravitational forces contribute well below this sensitivity [96]. The strongest current constraints of  $\alpha$  and  $\lambda$  obtained from (13.43) extend over a wide interaction range  $40 \text{ nm} < \lambda < 8 \text{ }\mu\text{m}$  (see the line labeled Casimir-less in Fig. 13.2).

Thus, Fig. 13.2 presents the strongest constraints on the Yukawa-type interaction obtained from Casimir physics. Almost all these constraints with except of the region

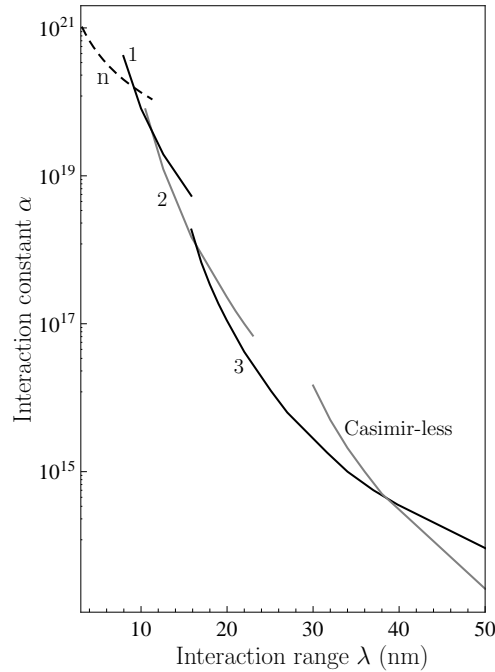


**Fig. 13.3** Constraints on the interaction constant  $\alpha$  of Yukawa-type interaction are shown as functions of the interaction range  $\lambda$  by the lines labeled n, 1, 2, 3, and Casimir-less, obtained from the experiments on neutron scattering, measuring the lateral and normal Casimir force between the sinusoidally corrugated surfaces, effective Casimir pressure, and from the Casimir-less experiment, respectively. The regions of  $(\lambda, \alpha)$  plane above each line are excluded and below are allowed

from 10 to 39 nm are obtained in [96] which is the fourth experiment discussed above. At  $\lambda = 8 \mu\text{m}$  the constraints found from the differential force measurements (which are also called the Casimir-less experiment) are of the same strength as the constraints found from the Cavendish-type experiments. At larger  $\lambda$  the strongest constraints are shown by a beginning of the line labeled gr reproduced from Fig. 13.1.

In Fig. 13.3 we reproduce the beginning of the line labeled Casimir-less in Fig. 13.2 on an enlarged scale in order to better demonstrate the constraints obtained in the range  $10 \text{ nm} < \lambda < 39 \text{ nm}$  [27, 28, 92, 95] from the experiments [27, 28, 90, 91, 93, 94] (i.e., from the first, second and third experiments discussed above). In this figure, the lines labeled n also indicate the strongest constraints on the Yukawa-type interaction obtained at  $\lambda < 10 \text{ nm}$  from the experiments on neutron scattering [97, 98] (in the region  $0.03 \text{ nm} < \lambda < 0.1 \text{ nm}$  the strongest constraints follow from the experiment using a pulsed neutron beam [99]).

There are also many other papers in the scientific literature devoted to constraining the Yukawa-type corrections to Newtonian gravity from the Casimir effect (see, e.g., [100, 101, 102, 103, 104]). The constraints obtained there are, however, somewhat weaker than the current strongest constraints presented in Figs. 13.2 and 13.3. It should be mentioned that in the range of extremely small  $\lambda$  the constraints on  $\alpha$

have been obtained from spectroscopic measurements in simple atomic systems like hydrogen and deuterium whose spectra can be calculated and measured with high precision. Thus, it was found that in the range  $2 \times 10^{-4} \text{ nm} < \lambda < 20 \text{ nm}$  the maximum strength of Yukawa interaction varies from  $2 \times 10^{27}$  to  $2 \times 10^{25}$  [105].

### 13.5 Dark Matter, Dark Energy and Their Hypothetical Constituents

According to astrophysical observations, the visible matter in the form of stars, galaxies, planets and radiation constitutes only about 5% of the total mass of the Universe. By studying stellar motion in the neighborhood of our galaxy ninety years ago, Oort found [106] that the galaxy mass must be much larger than the mass of all stars belonging to it. At the same time, an application of the virial theorem to the Coma cluster of galaxies by Zwicky [107] resulted in a much larger mass than that found by summing up the masses of all observed galaxies belonging to this cluster. In succeeding years, these results received ample recognition. Presently it is generally agreed that the dark matter, which reveals itself only gravitationally, is not composed of elementary particles of the Standard Model listed in Sect. 13.1 and adds up approximately 27% of the Universe energy.

The problem of what dark matter is remains unresolved. There are many approaches to its resolution which consider some hypothetical particles introduced in different theoretical schemes beyond the Standard Model as possible constituents of dark matter. Among these particles are axions, arions, massive neutrinos, weakly interacting massive particles (WIMP) etc. The possibility to explain the observational data by a modification of the gravitational theory in place of compensating for a deficiency in matter is also investigated. All these approaches are widely discussed in the literature [108, 109, 110, 111, 112].

During the last few years, the major support from astrophysics and cosmology was received by the model of cold dark matter. This model suggests that the constituents of dark matter are light particles which were produced at the first stages of the Universe evolution and became nonrelativistic long ago. The best candidate of this kind is a pseudoscalar Nambu-Goldstone boson called an axion.

This particle was introduced [78, 113, 114] for solving the problem of strong CP violation in quantum chromodynamics mentioned in Sect. 13.1, i.e., independently of the problem of dark matter. The point is that all the experimental data show that strong interactions are CP invariant and the electric dipole moment of a neutron is equal to zero. In contrast to these facts, the vacuum state of quantum chromodynamics depends on an angle  $\theta$  which violates the CP invariance and allows a nonzero electric dipole moment of a neutron. To resolve this contradiction between experiment and theory, Peccei and Quinn [78] introduced the new symmetry which received their names. In doing so the emergence of axions is a direct consequence of the violation of this symmetry [113, 114].

Later it was understood that axions and other axionlike particles arise in many extensions of the Standard Model. They can interact with particles of the Standard Model, e.g., with photons, electrons and nucleons, and lead to a number of processes which could be observed both in the laboratory experiments and in astrophysics and cosmology (see [108, 109, 110, 111, 112, 115, 116, 117, 118, 119, 120, 121] for a review). The question arises whether it is possible to constrain the parameters of axions from the Casimir effect. This question is considered below in Sects. 13.6 and 13.7.

Another unresolved problem of modern physics is the problem of dark energy. In the end of twentieth century, the observations of supernovae demonstrated that an expansion of the Universe is accelerating [122]. This fact is in some contradiction with expectations based on the general relativity theory and the properties of matter described by the Standard Model because the gravitational interaction of usual matter is attractive and should make the Universe expansion slower.

The concept of dark energy, i.e., some new kind of invisible matter which causes a repulsion, was introduced in numerous discussions of this problem. One approach to its resolution goes back to Einstein's cosmological constant which is closely connected with the problem of the quantum vacuum. According to the observational data, the dark energy constitutes as much as approximately 68% of the Universe energy. This corresponds to some background medium (physical vacuum) possessing the energy density of  $\epsilon \approx 10^{-9} \text{ J/m}^3$ . In order that this medium could accelerate the Universe expansion, it should possess the equation of state  $P = -\epsilon/3$ , i.e., the negative pressure.

The cosmological term  $\Lambda g_{ik}$ , where  $g_{ik}$  is the metrical tensor, when added to Einstein's equations of general relativity theory, results in just this equation of state. In doing so, the value of  $\Lambda$  is determined by the above value of  $\epsilon$  determined from the observed acceleration of the Universe expansion

$$\Lambda = 8\pi G\epsilon \approx 2 \times 10^{-52} \text{ m}^{-2}. \quad (13.44)$$

It was argued, however, that quantum field theory using a cutoff at the Planck momentum  $p_{Pl} = E_{Pl}/c$  leads to quite a different value of the vacuum energy density  $\epsilon_{vac} \approx 10^{11} \text{ J/m}^3$  which is different from  $\epsilon$  determined from observations by the factor of  $10^{120}$  [123, 124]. If to take into account that the vacuum energy density admits an interpretation in term of the cosmological constant [125], it becomes clear why this discrepancy by the factor of  $10^{120}$  was called the vacuum catastrophe [126].

Another approach to the understanding of dark energy attempts to model it by the fields and respective particles with unusual physical properties. One of the models of this kind introduces the real self-interacting scalar field  $\phi$  with a variable mass called chameleon [127]. The distinctive feature of chameleon particles is that they become heavier in more dense environments and lighter in free space.

Another model similar in spirit suggests that the interaction constant of the self-interacting real scalar field with usual matter depends on the density in the environment. The fields and particles of this kind are called symmetrons [128, 129, 130].

Symmetrons interact with usual matter described by the Standard Model weaker if the density of the environment is higher.

There are also other hypothetical particles which could lead to the negative pressure and help to understand the accelerating expansion of the Universe. For instance, the negative pressure originates from the Maxwell stress-energy tensor of massive photons in the Maxwell-Proca electrodynamics [131].

If the exotic particles, such as chameleons, symmetrons, massive photons etc., exist in nature, this should lead to some additional forces between the closely spaced macrobodies. In Sect. 13.8 the possibility of constraining these forces from measurements of the Casimir force is discussed.

### 13.6 Constraining Dark Matter Particles from the Casimir Effect

As was mentioned in previous section, the main candidate for the role of a dark matter particle is light pseudoscalar particle called an axion which can interact with photons, electrons, and nucleons. It can be easily seen that the interaction of axions with photons and electrons does not lead to sufficiently large forces between the closely spaced bodies which could be constrained from measurements of the Casimir force. These interactions of axions are investigated by other means. For example, the conversion process of photons into axions in strong magnetic field (the so-called Primakoff process) is used for an axion search in astrophysics [132] (see also reviews [117, 118, 119, 120] for already obtained constraints on interactions of axions with photons and electrons).

Here, we concentrate our attention on the interaction of axions with nucleons (neutrons and protons) which could lead to some noticeable additional force between two neighboring bodies. The interaction Lagrangian density between the originally introduced axion field  $a(x)$  and the fermionic field  $\psi(x)$  is given by [115, 118]

$$\mathcal{L}_{pv}(x) = \frac{g}{2m_a} \hbar^2 \bar{\psi}(x) \gamma_5 \gamma_\mu \psi(x) \partial^\mu a(x), \quad (13.45)$$

where  $g$  is the dimensionless interaction constant,  $m_a$  is the axion mass,  $\gamma_\mu$  with  $\mu = 0, 1, 2, 3$  and  $\gamma_5$  are the Dirac matrices. The Lagrangian density (13.45) is called pseudovector. It describes the interaction of fermions with pseudo Nambu-Goldstone bosons.

Various extensions of the Standard Model called the Grand Unified Theories (GUT) introduce the axionlike particles which interact with fermions through the pseudoscalar Lagrangian density [115, 118, 133]

$$\mathcal{L}_{ps}(x) = -ig\hbar c \bar{\psi}(x) \gamma_5 \psi(x) a(x). \quad (13.46)$$

Unlike (13.45), which contains a dimensional effective interaction constant  $g/m_a$ , the Lagrangian density (13.46) results in a renormalizable field theory.

When one considers an exchange of a single axion between two nucleons of mass  $m$  belonging to the closely spaced test bodies, both Lagrangian densities (13.45) and (13.46) lead to the common effective potential energy [134, 135]

$$V_{an}(r; \boldsymbol{\sigma}_1, \boldsymbol{\sigma}_2) = \frac{g^2 \hbar^3}{16\pi m^2 c} \left[ (\boldsymbol{\sigma}_1 \cdot \mathbf{n})(\boldsymbol{\sigma}_2 \cdot \mathbf{n}) \left( \frac{m_a^2 c^2}{\hbar^2 r} + \frac{3m_a c}{\hbar r^2} + \frac{3}{r^3} \right) - (\boldsymbol{\sigma}_1 \cdot \boldsymbol{\sigma}_2) \left( \frac{m_a c}{\hbar r^2} + \frac{1}{r^3} \right) \right], \quad (13.47)$$

where  $r = |\mathbf{r}_1 - \mathbf{r}_2|$  is a distance between nucleons,  $\boldsymbol{\sigma}_1, \boldsymbol{\sigma}_2$  are their spins, and  $\mathbf{n} = (\mathbf{r}_1 - \mathbf{r}_2)/r$  is the unit vector along the line connecting these nucleons.

The effective interaction energy (13.47) depends on the spins of nucleons and the respective force averages to zero after a summation over the volumes of unpolarized test bodies. Because of this, using (13.47), the parameters of axion  $g$  and  $m_a$  can not be constrained from experiments on measuring the Casimir force discussed in Sect. 13.2 (the possibilities of constraining the spin-dependent interactions are considered in the next section).

There is, however, the possibility to obtain the spin-independent interaction energy between two nucleons by considering the process of two-axion exchange. If the Lagrangian density (13.46) is used, the effective interaction energy is given by [83, 136, 137]

$$V_{aan}(r) = -\frac{g^4 \hbar^2}{32\pi^3 m^2} \frac{m_a}{r^2} K_1 \left( \frac{2m_a c r}{\hbar} \right), \quad (13.48)$$

where  $K_1(z)$  is the modified Bessel function of the second kind.

In the case of Lagrangian density (13.45), the respective field theory is non-renormalizable. As a result, the effective interaction energy between nucleons due to an exchange of two axions is not yet available (see [138] for more details). This means that measurements of the Casimir force can be used for constraining only the parameters of GUT axions described by the pseudoscalar Lagrangian density (13.46).

Similar to the cases of power-type and Yukawa-type interactions in (13.21) and (13.34), the hypothetical force between two experimental test bodies due to two-axion exchange of their nucleons is given by

$$F_{aan}(a) = -n_1 n_2 \frac{\partial}{\partial a} \int_{V_1} d^3 r_1 \int_{V_2} d^3 r_2 V_{aan}(|\mathbf{r}_1 - \mathbf{r}_2|), \quad (13.49)$$

where  $a$  is the closest distance between these bodies and  $n_1, n_2$  are the numbers of nucleons per unit volume of their materials.

We consider first a homogeneous Au sphere above a homogeneous Si plate of thickness  $D$  which is assumed to be infinitely large. Substituting (13.48) in (13.49) and using the integral representation [139]

$$\frac{K_1(z)}{z} = \int_1^\infty du \sqrt{u^2 - 1} e^{-zu}, \quad (13.50)$$

one obtains

$$F_{aan}^{SP}(a) = -\frac{\pi m_a \hbar^2}{m^2 m_H^2} C_1 C_2 \int_1^\infty du \frac{\sqrt{u^2 - 1}}{u} \left(1 - e^{-2m_a c u D / \hbar}\right) \times \int_a^{2R+a} [2R(z-a) - (z-a)^2] e^{-2m_a c u z / \hbar} dz. \quad (13.51)$$

Here, the coefficients  $C_1$  and  $C_2$  are defined for a sphere and a plate materials, respectively, in the following way:

$$C_{1,2} = \rho_{1,2} \frac{g_{an}^2}{4\pi} \left( \frac{Z_{1,2}}{\mu_{1,2}} + \frac{N_{1,2}}{\mu_{1,2}} \right), \quad (13.52)$$

where  $Z_{1,2}$  and  $N_{1,2}$  are the numbers of protons and the mean number of neutrons in the sphere and plate atoms, respectively, and  $\mu_{1,2} = m_{1,2}/m_H$  are defined as the mean masses of a sphere and a plate atoms divided by the mass of atomic hydrogen.

By integrating in (13.51) with respect to  $z$ , one obtains

$$F_{aan}^{SP}(a) = -\frac{\pi \hbar^4}{2m_a m^2 m_H^2 c^2} C_1 C_2 \int_1^\infty du \frac{\sqrt{u^2 - 1}}{u^3} e^{-2m_a c u a / \hbar} \times \left(1 - e^{-2m_a c u D / \hbar}\right) \chi\left(R, \frac{m_a c u}{\hbar}\right), \quad (13.53)$$

where the function  $\chi(r, z)$  similar to  $\Phi(r, \lambda)$  in (13.38) is defined as

$$\chi(r, z) = r - \frac{1}{2z} + \left(r + \frac{1}{2z}\right) e^{-4rz}. \quad (13.54)$$

The strongest constraints on the parameters of axionlike particles were obtained [140] from the differential measurements where the contribution of the Casimir force was nullified [96]. This experiment was already discussed in Sect. 13.4. Taking into account the structure of the plate consisting of Au and Si halves, as well as additional Cr and Au layers (see Sect. 13.4), and using (13.53), the differential force in the experimental configuration takes the form

$$F_{aan,Au}^{SP}(a) - F_{aan,Si}^{SP}(a) = -\frac{\pi \hbar^4}{2m_a m^2 m_H^2 c^2} (C_{Au} - C_{Si}) \int_1^\infty du \frac{\sqrt{u^2 - 1}}{u^3} \times e^{-2m_a c u (a + \tilde{\Delta}_2 + \Delta_1) / \hbar} \left(1 - e^{-2m_a c u D / \hbar}\right) X\left(\frac{m_a c u}{\hbar}\right), \quad (13.55)$$

where the following notation is introduced

$$X(z) = C_{Au} \left[ \chi(R, z) - e^{-2z\Delta_2} \chi(R - \Delta_2, z) \right] + C_{Cr} e^{-2z\Delta_2} \left[ \chi(R - \Delta_2, z) - e^{-2z\Delta_1} \chi(R - \Delta_2 - \Delta_1, z) \right] + C_s e^{-2z(\Delta_2 + \Delta_1)} \chi(R - \Delta_2 - \Delta_1, z) \quad (13.56)$$



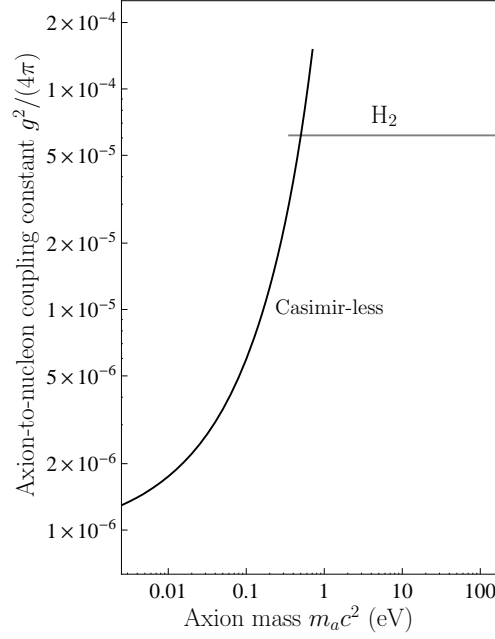


**Fig. 13.4** Constraints on the coupling constant  $g^2/(4\pi)$  of axions to nucleons are shown as functions of the axion mass  $m_a c^2$  by the lines labeled Casimir-less and  $H_2$  obtained from the Casimir-less experiment and from measuring dipole-dipole forces between protons in the beam of molecular hydrogen, respectively. The regions of  $[m_a c^2, g^2/(4\pi)]$  plane above each line are excluded and below are allowed

and the values of all coefficients  $C$  for Au, Cr, Si, and sapphire can be calculated by using (13.52) and numerical data for all involved quantities presented in [83].

The constraints on the parameters of hypothetical forces due to two-axion exchange between nucleons follow from the inequality

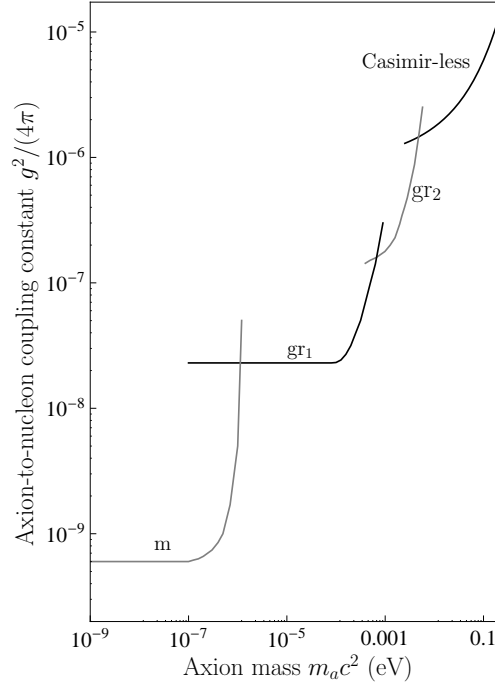
$$|F_{aan,Au}^{SP}(a) - F_{aan,Si}^{SP}(a)| \leq \Xi(a), \quad (13.57)$$

where  $\Xi(a)$  is the setup sensitivity to force differences in the experiment [96]. This inequality is similar to (13.43) used in constraining the interaction of Yukawa type. The strongest current constraints on the coupling constant of axions to nucleons  $g$  follow from (13.57) in the region of axion masses  $4.9 \text{ meV} < m_a c^2 < 0.5 \text{ eV}$ .

In Fig. 13.4 the obtained constraints are shown by the line labeled Casimir-less. Similar to all previous figures, the values of axion parameters belonging to the area of  $[m_a c^2, g^2/(4\pi)]$  plane above the line are excluded by the results of differential force measurements whereas the plane area below the line is allowed.

For  $m_a c^2 > 0.5 \text{ eV}$  the strongest current constraints on  $g$  are obtained by comparing with theory the measurement results for the dipole-dipole forces between two protons in the beam of molecular hydrogen [141, 142]. They are shown by the line labeled  $H_2$  in Fig. 13.4. In this experiment, the additional force between protons arises

**Fig. 13.5** Constraints on the coupling constant  $g^2/(4\pi)$  of axions to nucleons are shown as functions of the axion mass  $m_a c^2$  by the lines labeled m,  $gr_1$ ,  $gr_2$ , and Casimir-less obtained from the magnetometer measurements, Cavendish-type experiment, measuring the minimum force of gravitational strength, and from the Casimir-less experiment, respectively. The regions of  $[m_a c^2, g^2/(4\pi)]$  plane above each line are excluded and below are allowed



due to an exchange of one axion and is described by the spin-dependent interaction energy (13.47). As a result, for sufficiently large  $m_a$  the obtained constraints on  $g$  are much stronger than those found from the differential force measurements. What is more, the constraints of line  $H_2$  are valid both for the originally introduced axions whose interaction with nucleons is described by the Lagrangian density (13.45) and for axionlike particles with respective Lagrangian density (13.46).

In the region of axion masses  $m_a c^2 < 4.9$  meV the strongest constraints of  $g$  follow from gravitational experiments. In Fig. 13.5, the line labeled  $gr_1$  shows the constraints on  $g$  found [71] from the Cavendish-type experiment [70]. These constraints are the strongest ones in the region of axion masses  $1 \mu\text{eV} < m_a c^2 < 0.676$  meV. Within the relatively short range of axion masses  $0.676 \text{ meV} < m_a c^2 < 4.9$  meV the strongest constraints were obtained [138] by using the planar torsional oscillator for measuring the minimum force of gravitational strength [143, 144]. The respective constraints are shown by the line labeled  $gr_2$  in Fig. 13.5. The gravitational constraints shown by the lines  $gr_1$  and  $gr_2$  are valid for only the axionlike particles whose interaction with nucleons is described by the Lagrangian density (13.46) because in the gravitational experiments the test bodies used are unpolarized.

For the smallest axion masses  $m_a c^2 < 1 \mu\text{eV}$ , the strongest constraints on  $g$  were again obtained from considering the spin-dependent forces which arise due to a one-axion exchange in the comagnetometer measurements using the spin-polarized K and  $^3\text{He}$  atoms and the  $^3\text{He}$  spin source [145]. These constraints are shown by the line labeled m in Fig. 13.5. They are valid for all types of axions and axionlike particles.

The competitive constraints on the parameters of axionlike particles were obtained also from several other experiments on measuring the Casimir interaction (see, e.g., [103, 104, 146, 147, 148, 149, 150, 151]). They are, however, weaker than those shown by the line labeled Casimir-less and  $\text{H}_2$  in Fig. 13.4.

### 13.7 Could the Casimir Effect be Used For Testing Spin-Dependent Interactions?

As explained in the previous section, the process of one-axion exchange between two nucleons described by the pseudovector Lagrangian density (13.45) results in the spin-dependent interaction energy (13.47) which does not lead to any additional force between two unpolarized test bodies. The parameters of originally introduced axions described by this interaction energy were constrained using, e.g., the magnetometer measurements or from measuring dipole-dipole forces between protons (see Sect. 13.6).

There are also other predictions of spin-dependent interactions beyond the Standard Model. In fact the coupling constant of axions to nucleons considered above describes either the pseudoscalar or pseudovector interactions. This can be notated as  $g \equiv g_P$ . In addition to the one-axion exchange, it is possible to consider an exchange of one light vector particle between two nucleons with a vector and axial vector couplings. This corresponds to the following Lagrangian density:

$$\mathcal{L}_{VA}(x) = \hbar c \bar{\psi}(x) \gamma^\mu (g_V + g_A \gamma_5) \psi(x) A_\mu(x). \quad (13.58)$$

This Lagrangian density results in the effective spin-dependent interaction energies between two nucleons [145]

$$V_1(r) = \frac{g_A^2}{4\pi r} \hbar (\boldsymbol{\sigma}_1 \cdot \boldsymbol{\sigma}_2) e^{-m_A c r / \hbar} \quad (13.59)$$

or

$$V_2(r) = -\frac{g_A g_V}{4\pi m} \hbar^2 ([\boldsymbol{\sigma}_1 \times \boldsymbol{\sigma}_2] \cdot \mathbf{n}) \left( \frac{m_A c}{\hbar r} + \frac{1}{r^2} \right) e^{-m_A c r / \hbar}, \quad (13.60)$$

where  $m_A$  is the mass of a vector field  $A_\mu$ . The parameters of the interaction energies (13.59) and (13.60) were constrained by the same comagnetometer measurements [145] which have already been used in Sect. 13.6 for constraining the interaction energy (13.47).

Below we discuss the possibility of constraining the spin-dependent interaction energy (13.47) from measuring the effective Casimir pressure. For this purpose it was proposed [152] to use the Casimir plates made of silicon carbide (SiC) with aligned nuclear spins. It has been known that the nuclear spin of  $^{29}\text{Si}$  is equal to  $1/2$  owing to the presence of one neutron with an uncompensated spin. In native Si there is only 4.68% of the isotope  $^{29}\text{Si}$ . In nanotechnology, however, the special procedures are elaborated for growing the isotopically controlled bulk Si [153].

In [152] it was assumed that a fraction of Si atoms  $\kappa$  in both plates is polarized in some definite direction due to the polarization of their nuclear spins (it was shown that an additional force due to the electronic polarization does not permit to obtain competitive constraints on the coupling constant of axions to electrons). In order to obtain the nonzero additional force between plates due to one-axion exchange, the atomic polarization should be perpendicular to the plates and directed either in one direction or in the opposite directions [152].

Under these conditions, by integrating the interaction energy (13.47) over the volumes of two parallel plates of density  $\rho$  and thickness  $D$ , for the force per unit area of the plates (i.e., pressure) one obtains [152]

$$P_{an}(a) = \pm g^2 \frac{\kappa^2 \rho^2 \hbar^3}{8m^2 m_{\text{H}}^2 c} e^{-m_a c a / \hbar} \left(1 - e^{-m_a c D / \hbar}\right)^2. \quad (13.61)$$

The force (13.61) could be constrained from the experiments [27, 28] on measuring the effective Casimir pressure using a micromechanical torsional oscillator if the test bodies were made of SiC with aligned nuclear spins. Similar to (13.41), in this case the constraints are obtained from the inequality

$$|P_{an}(a)| \leq \Delta P(a). \quad (13.62)$$

For the pressure (13.61), the strongest constraints follow at  $a = 300$  nm, where  $\Delta P(a) = 0.22$  mPa [27, 28], under the conditions that  $\kappa = 1$  and  $D \gg \hbar / (m_a c)$ , i.e., the plates are sufficiently thick. The density of SiC is  $\rho = 3.21$  g/cm<sup>3</sup>. The most strong constraint that can be placed in this way on axions and axionlike particles with  $m_a = 0.0126$  eV is  $g^2 / (4\pi) \leq 4.43 \times 10^{-5}$  [152], which is weaker than that found from the Casimir-less experiment (see Fig. 13.4) but is applicable to all kinds of axions.

An experiment on measuring the Casimir pressure between parallel plates with aligned nuclear spins can be also used for constraining the interaction of axions with nucleons from a simultaneous account of one- and two-axion exchange. In this case the constraints are obtained from the inequality

$$|P_{an}(a) + P_{aan}(a)| \leq \Delta P(a). \quad (13.63)$$

Here the additional pressure between two thick plates due to one-axion exchange is given by (13.61), where the last factor on the right-hand side is replaced with unity, and  $P_{aan}$  is obtained by integration of the interaction energy (13.48) over the volumes of both plates

$$P_{aan}(a) = -\frac{C_{\text{SiC}}^2 \hbar^3}{2m^2 m_{\text{H}}^2 c} \int_1^\infty du \frac{\sqrt{u^2 - 1}}{u^2} e^{-2m_a c a u / \hbar}. \quad (13.64)$$

The constant  $C_{\text{SiC}}$  is defined as in (13.52) using the numerical data presented in [83].

It has been shown [152] that using (13.63) in the region of axion masses below 1 eV one could obtain up to an order of magnitude stronger constraints on the coupling of axions with nucleons than from (13.62). These constraints, however, would be valid only for the GUT axions which interaction with nucleons is described by the pseudoscalar Lagrangian density (13.46).

### 13.8 Constraining Dark Energy Particles from the Casimir Effect

Axions considered above as the most probable constituents of dark matter are the Nambu-Goldstone bosons, which appear in the formalism of quantum field theory when some symmetry (in this case the Peccei-Quinn symmetry) is broken both spontaneously (i.e., the vacuum is not invariant) and dynamically (i.e., in the Lagrangian). Although these particles are not the part of the Standard Model, they can be considered as its natural supplement. The axionlike particles introduced later also fall into the standard pattern of quantum field theory.

The particles proposed as the possible constituents of dark energy (chameleons, symmetrons, etc., see Sect. 13.5) are quite different. Unlike all conventional elementary particles, the properties of these particles depend on the environmental conditions.

We begin with chameleons whose mass is larger, i.e., the interaction range is shorter, in environments with higher energy density (see Sect. 13.5). Mathematically chameleons are described by the real self-interacting scalar field  $\Phi$  possessing a variable mass. In the static case, this field satisfies the simplest equation of the form [127, 154]:

$$\Delta\Phi = \frac{1}{(\hbar c)^4} \frac{\partial V(\Phi)}{\partial\Phi} + \frac{\rho}{M} e^{\hbar\Phi/(Mc)}, \quad (13.65)$$

where  $M$  is the typical mass of conventional particles forming the background matter of density  $\rho$  and  $V(\Phi)$  is the self-interaction which decreases monotonically with increasing  $\Phi$ .

An interaction between chameleons and background matter with density  $\rho$  in (13.65) implies that the effective interaction potential describing the chameleon field is given by

$$V_{\text{eff}}(\Phi) = V(\Phi) + \rho \hbar^3 c^5 e^{\hbar\Phi/(Mc)}. \quad (13.66)$$

Although the self-interaction  $V$  is assumed to be monotonic, this effective potential takes the minimum value for  $\Phi_0$  satisfying the condition

$$\frac{\partial V(\Phi_0)}{\partial\Phi} + \frac{\rho(\hbar c)^4}{M} e^{\hbar\Phi_0/(Mc)} = 0. \quad (13.67)$$

Then the mass of the field  $\Phi_0$  is given by

$$m_{\Phi_0}^2 \equiv \frac{1}{\hbar^2 c^6} \frac{\partial^2 V_{\text{eff}}(\Phi_0)}{\partial \Phi^2} = \frac{1}{\hbar^2 c^6} \frac{\partial^2 V(\Phi_0)}{\partial \Phi^2} + \frac{\rho}{M^2} \left( \frac{\hbar}{c} \right)^3 e^{\hbar \Phi_0 / (Mc)} \quad (13.68)$$

and depends on the background mass density  $\rho$ .

According to the above assumption,  $V$  is a decreasing function of  $\Phi$ . Then,  $\partial V / \partial \Phi$  is negative and monotonously increasing whereas  $\partial^2 V / \partial \Phi^2$  is positive and decreasing. According to (13.68), this means that we have larger  $m_{\Phi_0}$  and smaller  $\Phi_0$  for larger values of the background mass density  $\rho$  [127].

There are different possible forms of the chameleon self-interaction suggested in the literature [127, 154, 155], e.g.,

$$V(\Phi) = E^4 \left( \frac{E}{\hbar c \Phi} \right)^n, \quad V(\Phi) = E_0^4 e^{E^n / (\hbar c \Phi)^n} \quad (13.69)$$

or

$$V(\Phi) = E_0^4 \left[ 1 + \left( \frac{E}{\hbar c \Phi} \right)^n \right], \quad (13.70)$$

where  $E_0$  and  $E$  are the quantities with a dimension of energy and  $n = 1, 2, 3$ , etc. According to [154], if the chameleon field is responsible for the presently observed acceleration of the Universe, it should be  $E_0 \approx 2.4 \times 10^{-12}$  GeV.

Similar to axions, an exchange of chameleons between two constituent particles of two closely spaced test bodies results in some additional force. The constraints on this force can be obtained from experiments on measuring the Casimir force [154]. In this case, however, both the additional force and constraints on it strongly depend not only on the specific experimental setup but also on the form of chameleon self-interaction and other related parameters (see [154, 155, 156] for some specific results obtained in the configuration of two parallel plates and a sphere above a plate with different models of self-interaction).

Another hypothetical particle mentioned in Sect. 13.5 as a possible constituent of dark energy is a symmetron whose interaction with usual matter becomes weaker with increasing mass density of the environment [128, 129]. In the static case the symmetron field  $\Phi_s$  satisfies the equation [128, 129, 130]

$$\Delta \Phi_s = \frac{1}{(\hbar c)^4} \frac{\partial V^s(\Phi_s)}{\partial \Phi_s} + \left[ \frac{\hbar}{c} \frac{\rho}{M^2} - \left( \frac{\mu c}{\hbar} \right)^2 \right] \Phi_s, \quad (13.71)$$

where  $V^s$  is the symmetron self-interaction and  $\mu$  is the symmetron mass.

The respective effective potential leading to the right-hand side of (13.71) is given by [130]

$$V_{\text{eff}}^s(\Phi_s) = V^s(\Phi_s) + \frac{1}{2} (\hbar c)^4 \left[ \frac{\hbar}{c} \frac{\rho}{M^2} - \left( \frac{\mu c}{\hbar} \right)^2 \right] \Phi_s^2, \quad (13.72)$$

where the self-interaction of a symmetron field takes the standard form

$$V^s(\Phi_s) = \frac{1}{4}\lambda\Phi_s^4, \quad (13.73)$$

and  $\lambda$  is a dimensionless constant.

The effective potential (13.72), (13.73) takes the minimum value for  $\Phi_s = \Phi_{s,0}$  satisfying the condition

$$\lambda\Phi_{s,0}^3 + (\hbar c)^4 \left[ \frac{\hbar}{c} \frac{\rho}{M^2} - \left( \frac{\mu c}{\hbar} \right)^2 \right] \Phi_{s,0} = 0. \quad (13.74)$$

If the density of background matter  $\rho < \rho_0 = c^3 M^2 \mu^2 / \hbar^3$ , the minimum value of  $V_{\text{eff}}^s$  is attained at

$$\Phi_{s,0} = \frac{(\hbar c)^2}{\sqrt{\lambda}} \left[ \left( \frac{\mu c}{\hbar} \right)^2 - \frac{\hbar}{c} \frac{\rho}{M^2} \right]^{1/2}. \quad (13.75)$$

Under the opposite condition  $\rho > \rho_0$ , the minimum value of  $V_{\text{eff}}^s$  is at  $\Phi_{s,0} = 0$ . Thus, if  $\rho < \rho_0$  the reflection symmetry is broken and the vacuum expectation value of  $\Phi_{s,0}$  takes a nonzero value. By contrast, in the regions of high density of background matter  $\rho > \rho_0$ , the vacuum expectation value of  $\Phi_{s,0}$  turns into zero.

The exchange of symmetrons between two closely spaced material bodies results in some additional force which was calculated in [157] for the experimental configurations of two parallel plates and a sphere above a plate. According to the results of [157], strong constraints on the parameters of a symmetron can be obtained from measurements of the Casimir force in these configurations. These measurements, however, are not yet performed. Prospects in constraining various hypothetical interactions beyond the Standard Model and some other laboratory experiments are discussed in the next section.

### 13.9 Outlook

Many experiments on measuring the Casimir interaction mentioned above were performed entirely in an effort to investigate the Casimir effect. This means that the constraints on corrections to Newtonian gravity and axionlike particles discussed above were obtained as some kind of by-product. In [158] some improvements in the configurations of experiments employing both smooth and sinusoidally corrugated surfaces of a sphere and a plate were suggested which allow obtaining up to an order of magnitude stronger constraints. Specifically, for the configurations with corrugated surfaces this could be reached by using smaller corrugation periods and larger corrugation amplitudes [158].

There are many proposals of new Casimir experiments aimed for testing gravity and predictions beyond the Standard Model at short distances. Thus, it is suggested to measure the Casimir pressure between two parallel plates at separations up to 10–20  $\mu\text{m}$  (Casimir and Non-Newtonian Force Experiment called CANNEX) [159, 160, 161, 162, 163]. This experiment promises obtaining stronger constraints not only on

non-Newtonian gravity and axionlike particles, but also on chameleon, symmetron and some other theoretical predictions beyond the Standard Model.

The Casimir-Polder interaction between two atoms or an atom and a cavity wall can also be used for constraining the hypothetical interactions. The constraints on an axion to nucleon coupling constant obtained in this way [146] were mentioned in Sect. 13.6. In [164] it was suggested to measure the Casimir-Polder force between a Rb atom and a movable Si plate screened with an Au film. This makes it possible to strengthen constraints on the Yukawa interaction constant  $\alpha$  in the interaction range around  $1 \mu\text{m}$ . According to [165], the measured deviations of the Casimir-Polder force between two polarized particles, arising for photons of nonzero mass, from the standard one calculated for massless photons can be used for constraining the extradimensional unification models.

An interesting method for detecting the interaction of axion with nucleons by means of a levitated optomechanical system was suggested in [166]. In fact this is a version of the Casimir-less experiment [96] where the contribution of the Casimir force is nullified (see Sects. 13.4 and 13.6). The suggested method could further strengthen the already obtained constraints on the coupling constant of axions to nucleons and on the Yukawa-type corrections to Newtonian gravity.

There are also many proposed laboratory experiments which are not closely related to the Casimir physics but could lead to constraints on the hypothetical interactions in the same or neighboring regions of parameters as the Casimir effect. Some of them are discussed below.

Thus, the neutron interferometry already used for constraining the Yukawa-type forces (see Sect. 13.4) has large potential for improving the obtained constraints. Several experiments of this kind have been performed and suggested pursuing this goal (see, e.g., [167, 168, 169, 170, 171]).

There is a continuing interest in the literature to constraining the power-type, Yukawa-type and other hypothetical interactions by means of atomic and molecular spectroscopy. A few experiments of this kind await for their realization [172, 173, 174].

It has been known that the levitated nanoparticle sensors are sensitive to the static forces down to  $10^{-17}$  N. In [175] it was suggested to use such sensors for obtaining constraints on the Yukawa-type corrections to Newtonian gravity. The optomechanical methods exploiting the levitated sensors were proposed also for constraining the hypothetical interaction of Yukawa type [176].

Recent literature also contains information on already performed experiment constraining the exotic interaction between moving polarized electrons and unpolarized nucleons by means of a magnetic force microscope [177], on the general scheme allowing an extraction of constraints on any specific model from different experiments [178], and on a compressed ultrafast photography system using temporal lensing for probing short-range gravity [179].

Interest in all these topics has quickened in the past few years. One may expect that measurements of the Casimir force and related table-top laboratory experiments will



furnish insights into the nature of some theoretical predictions beyond the Standard Model and their relationship to reality.

**Acknowledgments** This is a preprint of the following chapter: Galina L. Klimchitskaya and Vladimir M. Mostepanenko, Testing Gravity and Predictions Beyond the Standard Model at Short Distances: The Casimir Effect, published in *Modified and Quantum Gravity, From Theory to Experimental Searches on All Scales*, edited by Christian Pfeifer, Claus Lämmerzahl, 2023, Springer, reproduced with permission of Springer. The final authenticated version is available online at: <https://doi.org/10.1007/978-3-031-31520-6>. G.L.K. was partially funded by the Ministry of Science and Higher Education of Russian Federation ("The World-Class Research Center: Advanced Digital Technologies," contract No. 075-15-2022-311 dated April 20, 2022). The research of V.M.M. was partially carried out in accordance with the Strategic Academic Leadership Program "Priority 2030" of the Kazan Federal University.

## References

1. Wald, R.M.: *General Relativity*. University of Chicago Press, Chicago (2010)
2. Weinberg, S.: *Gravitation and Cosmology: Principles and Applications of the General Theory of Relativity*. Wiley, New York (1972)
3. Jackson, J.D.: *Classical Electrodynamics*. Wiley, New York (1998)
4. Feynman, R.P.: *Quantum Electrodynamics*. Westview Press, Boulder (1998)
5. Renton, P.: *Electroweak Interactions. An Introduction to the Physics of Quarks and Leptons*. Cambridge University Press, Cambridge (1990)
6. Greiner, W., Schramm, S., Stein, E.: *Quantum Chromodynamics*. Springer, Berlin (2007)
7. Burgess, C., Moore, G.: *The Standard Model*. Cambridge University Press, Cambridge (2011)
8. Wess, J., Bagger, J.: *Supersymmetry and Supergravity*. Princeton University Press, Princeton (1992)
9. Zwiebach, B.: *A First Course in String Theory*. Cambridge University Press, Cambridge (2006)
10. Casimir, H.B.G.: On the attraction between two perfectly conducting plates. *Proc. K. Ned. Akad. Wet. B* **51**, 793–795 (1948)
11. Erdélyi, A., Magnus, W., Oberhettinger, F.G.: *Higher Transcendental Functions*, Vol. 1. Krieger, New York (1981)
12. Lifshitz, E.M.: The theory of molecular attractive forces between solids. *Zh. Eksp. Teor. Fiz.* **29**, 94–110 (1955); *Sov. Phys. JETP* **2**, 73–83 (1956)
13. Richmond, P., Ninham, B.W.: A note on the extension of the Lifshitz theory of van der Waals forces to magnetic media. *J. Phys. C: Solid State Phys.* **4**, 1988–1993 (1971)
14. Bordag, M., Klimchitskaya, G.L., Mohideen, U., Mostepanenko, V.M.: *Advances in the Casimir Effect*. Oxford University Press, Oxford (2015)
15. Klimchitskaya, G.L., Mohideen, U., Mostepanenko, V.M.: The Casimir force between real materials: Experiment and theory. *Rev. Mod. Phys.* **81**, 1827–1885 (2009)
16. Canaguier-Durand, A., Maia Neto, P.A., Cervero-Pelaez, I., Lambrecht, A., Reynaud, S.: Casimir Interaction between Plane and Spherical Metallic Surfaces. *Phys. Rev. Lett.* **102**, 230404 (2009)
17. Hartmann, M., Ingold, G.-L., Maia Neto, P.A.: Plasma versus Drude Modeling of the Casimir Force: Beyond the Proximity Force Approximation. *Phys. Rev. Lett.* **119**, 043901 (2017)

18. Spreng, B., Hartmann, M., Henning, V., Maia Neto, P.A., Ingold, G.-L.: Proximity force approximation and specular reflection: Application of the WKB limit of Mie scattering to the Casimir effect. *Phys. Rev. A* **97**, 062504 (2018)
19. Hartmann, M., Ingold, G.-L., Maia Neto, P.A.: Advancing numerics for the Casimir effect to experimentally relevant aspect ratios. *Phys. Scr.* **93**, 114003 (2018)
20. Fosco, C.D., Lombardo, F.C., Mazzitelli, F.D.: Proximity force approximation for the Casimir energy as a derivative expansion. *Phys. Rev. D* **84**, 105031 (2011)
21. Bimonte, G., Emig, T., Jaffe, R.L., Kardar, M.: Casimir forces beyond the proximity force approximation. *Europhys. Lett.* **97**, 50001 (2012)
22. Bimonte, G., Emig, T., Kardar, M.: Material dependence of Casimir force: gradient expansion beyond proximity. *Appl. Phys. Lett.* **100**, 074110 (2012)
23. Teo, L.P.: Material dependence of Casimir interaction between a sphere and a plate: First analytic correction beyond proximity force approximation. *Phys. Rev. D* **88**, 045019 (2013)
24. Bimonte, G.: Going beyond PFA: A precise formula for the sphere-plate Casimir force. *Europhys. Lett.* **118**, 20002 (2017)
25. Decca, R.S., Fischbach, E., Klimchitskaya, G.L., Krause, D.E., López, D., Mostepanenko, V.M.: Improved tests of extra-dimensional physics and thermal quantum field theory from new Casimir force measurements. *Phys. Rev. D* **68**, 116003 (2003)
26. Decca, R.S., López, D., Fischbach, E., Klimchitskaya, G.L., Krause, D.E., Mostepanenko, V.M.: Precise comparison of theory and new experiment for the Casimir force leads to stronger constraints on thermal quantum effects and long-range interactions. *Ann. Phys. (N.Y.)* **318**, 37–80 (2005)
27. Decca, R.S., López, D., Fischbach, E., Klimchitskaya, G.L., Krause, D.E., Mostepanenko, V.M.: Tests of new physics from precise measurements of the Casimir pressure between two gold-coated plates. *Phys. Rev. D* **75**, 077101 (2007)
28. Decca, R.S., López, D., Fischbach, E., Klimchitskaya, G.L., Krause, D.E., Mostepanenko, V.M.: Novel constraints on light elementary particles and extra-dimensional physics from the Casimir effect. *Eur. Phys. J. C* **51**, 963–975 (2007)
29. Chang, C.-C., Banishev, A.A., Castillo-Garza, R., Klimchitskaya, G.L., Mostepanenko, V.M., Mohideen, U.: Gradient of the Casimir force between Au surfaces of a sphere and a plate measured using an atomic force microscope in a frequency-shift technique. *Phys. Rev. B* **85**, 165443 (2012)
30. Xu, J., Klimchitskaya, G.L., Mostepanenko, V.M., Mohideen, U.: Reducing detrimental electrostatic effects in Casimir-force measurements and Casimir-force-based microdevices. *Phys. Rev. A* **97**, 032501 (2018)
31. Liu, M., Xu, J., Klimchitskaya, G.L., Mostepanenko, V.M., Mohideen, U.: Examining the Casimir puzzle with an upgraded AFM-based technique and advanced surface cleaning. *Phys. Rev. B* **100**, 081406(R) (2019)
32. Liu, M., Xu, J., Klimchitskaya, G.L., Mostepanenko, V.M., Mohideen, U.: Precision measurements of the gradient of the Casimir force between ultraclean metallic surfaces at larger separations. *Phys. Rev. A* **100**, 052511 (2019)
33. Bimonte, G., Spreng, B., Maia Neto, P.A., Ingold, G.-L., Klimchitskaya, G.L., Mostepanenko, V.M., Decca, R.S.: Measurement of the Casimir Force between 0.2 and 8  $\mu\text{m}$ : Experimental Procedures and Comparison with Theory. *Universe* **7**, 93 (2021)
34. Banishev, A.A., Chang, C.-C., Klimchitskaya, G.L., Mostepanenko, V.M., Mohideen, U.: Measurement of the gradient of the Casimir force between a nonmagnetic gold sphere and a magnetic nickel plate. *Phys. Rev. B* **85**, 195422 (2012)
35. Banishev, A.A., Klimchitskaya, G.L., Mostepanenko, V.M., Mohideen, U.: Demonstration of the Casimir Force between Ferromagnetic Surfaces of a Ni-Coated Sphere and a Ni-Coated Plate. *Phys. Rev. Lett.* **110**, 137401 (2013)
36. Banishev, A.A., Klimchitskaya, G.L., Mostepanenko, V.M., Mohideen, U.: Casimir interaction between two magnetic metals in comparison with nonmagnetic test bodies. *Phys. Rev. B* **88**, 155410 (2013)
37. Bimonte, G., López, D., Decca, R.S.: Isoelectronic determination of the thermal Casimir force. *Phys. Rev. B* **93**, 184434 (2016)

38. Bezerra, V.B., Klimchitskaya, G.L., Mostepanenko, V.M., Romero, C.: Violation of the Nernst heat theorem in the theory of thermal Casimir force between Drude metals. *Phys. Rev. A* **69**, 022119 (2004)
39. Bordag, M., Pirozhenko, I.: Casimir entropy for a ball in front of a plane. *Phys. Rev. D* **82**, 125016 (2010)
40. Klimchitskaya, G.L., Mostepanenko, V.M.: Low-temperature behavior of the Casimir free energy and entropy of metallic films. *Phys. Rev. A* **95**, 012130 (2017)
41. Klimchitskaya, G.L., Korikov, C.C.: Analytic results for the Casimir free energy between ferromagnetic metals. *Phys. Rev. A* **91**, 032119 (2015)
42. Castro Neto, A.H., Guinea, F., Peres, N.M.R., Novoselov, K.S., Geim, A.K.: The electronic properties of graphene. *Rev. Mod. Phys.* **81**, 109–162 (2009)
43. Bordag, M., Klimchitskaya, G.L., Mostepanenko, V.M., Petrov, V.M.: Quantum field theoretical description for the reflectivity of graphene. *Phys. Rev. D* **91**, 045037 (2015); Erratum in **93**, 089907 (2016)
44. Bordag, M., Fialkovskiy, I., Vassilevich, D.: Enhanced Casimir effect for doped graphene. *Phys. Rev. B* **93**, 075414 (2016); Erratum in **95**, 119905 (2017)
45. Klimchitskaya, G.L., Mostepanenko, V.M., Sernelius, Bo E.: Two approaches for describing the Casimir interaction with graphene: Density-density correlation function versus polarization tensor. *Phys. Rev. B* **89**, 125407 (2014)
46. Klimchitskaya, G.L., Mostepanenko, V.M.: Conductivity of pure graphene: Theoretical approach using the polarization tensor. *Phys. Rev. B* **93**, 245419 (2016)
47. Banishev, A.A., Wen, H., Xu, J., Kawakami, R.K., Klimchitskaya, G.L., Mostepanenko, V.M., Mohideen, U.: Measuring the Casimir force gradient from graphene on a SiO<sub>2</sub> substrate. *Phys. Rev. B* **87**, 205433 (2013)
48. Klimchitskaya, G.L., Mohideen, U., Mostepanenko, V.M.: Theory of the Casimir interaction for graphene-coated substrates using the polarization tensor and comparison with experiment. *Phys. Rev. B* **89**, 115419 (2014)
49. Liu, M., Zhang, Y., Klimchitskaya, G.L., Mostepanenko, V.M., Mohideen, U.: Demonstration of an Unusual Thermal Effect in the Casimir Force from Graphene. *Phys. Rev. Lett.* **126**, 206802 (2021)
50. Liu, M., Zhang, Y., Klimchitskaya, G.L., Mostepanenko, V.M., Mohideen, U.: Experimental and theoretical investigation of the thermal effect in the Casimir interaction from graphene. *Phys. Rev. B* **104**, 085436 (2021)
51. Bezerra, V.B., Klimchitskaya, G.L., Mostepanenko, V.M., Romero, C.: Nernst heat theorem for the thermal Casimir interaction between two graphene sheets. *Phys. Rev. A* **94**, 042501 (2016)
52. Klimchitskaya G.L., Mostepanenko, V.M.: Low-temperature behavior of the Casimir-Polder free energy and entropy for an atom interacting with graphene. *Phys. Rev. A* **98**, 032506 (2018)
53. Klimchitskaya G.L., Mostepanenko V.M.: Nernst heat theorem for an atom interacting with graphene: Dirac model with nonzero energy gap and chemical potential. *Phys. Rev. D* **101**, 116003 (2020)
54. Klimchitskaya G.L., Mostepanenko V.M.: Quantum field theoretical description of the Casimir effect between two real graphene sheets and thermodynamics. *Phys. Rev. D* **102**, 016006 (2020)
55. Klimchitskaya, G.L., Mostepanenko V.M.: Casimir and Casimir-Polder Forces in Graphene Systems: Quantum Field Theoretical Description and Thermodynamics. *Universe* **6**, 150 (2020)
56. Klimchitskaya G.L., Mostepanenko V.M.: An alternative response to the off-shell quantum fluctuations: a step forward in resolution of the Casimir puzzle. *Eur. Phys. J. C* **80**, 900 (2020)
57. Klimchitskaya G.L., Mostepanenko V.M.: Theory-experiment comparison for the Casimir force between metallic test bodies: A spatially nonlocal dielectric response. *Phys. Rev. A* **105**, 012805 (2022)
58. Klimchitskaya G.L., Mostepanenko V.M.: Casimir entropy and nonlocal response functions to the off-shell quantum fluctuations. *Phys. Rev. D* **103**, 096007 (2021)

59. Klimchitskaya G.L., Mostepanenko V.M.: Casimir effect for magnetic media: Spatially non-local response to the off-shell quantum fluctuations. *Phys. Rev. D* **104**, 085001 (2021)
60. Mostepanenko, V.M.: Casimir Puzzle and Casimir Conundrum: Discovery and Search for Resolution. *Universe* **7**, 84 (2021).
61. Anselm, A.A., Uraltsev, N.G.: A second massless axion? *Phys. Lett. B* **114**, 39–41 (1982)
62. Mostepanenko, V.M., Sokolov, I.Yu.: Restrictions on long-range forces following from the Casimir effect. *Yadern. Fiz.* **46**, 1174–1180 (1987); *Sov. J. Nucl. Phys.* **46**, 685–688 (1987)
63. Feinberg, G., Sucher, J.: Long-Range Forces from Neutrino-Pair Exchange. *Phys. Rev.* **166**, 1638–1644 (1968)
64. Fischbach, E.: Long-range forces and neutrino mass. *Ann. Phys. (N.Y.)* **247**, 213–291 (1996)
65. Deser, S., Zumino, B.: Broken Supersymmetry and Supergravity. *Phys. Rev. Lett.* **38**, 1433–1436 (1977)
66. Randall, L., Sundrum, R.: Large Mass Hierarchy from a Small Extra Dimension. *Phys. Rev. Lett.* **83**, 3370–3373 (1999)
67. Randall, L., Sundrum, R.: An Alternative to Compactification. *Phys. Rev. Lett.* **83**, 4690–4693 (1999)
68. Gundlach, J.H., Smith, G.L., Adelberger, E.G., Heckel, B.R., Swanson, H.E.: Short-Range Test of the Equivalence Principle. *Phys. Rev. Lett.* **78**, 2523–2526 (1997)
69. Smith, G.L., Hoyle, C.D., Gundlach, J.H., Adelberger, E.G., Heckel, B.R., Swanson, H.E.: Short-range tests of the equivalence principle. *Phys. Rev. D* **61**, 022001 (2000)
70. Kapner, D.J., Cook, T.S., Adelberger, E.G., Gundlach, J.H., Heckel, B.R., Hoyle, C.D., Swanson, H.E.: Tests of the Gravitational Inverse-Square Law below the Dark-Energy Length Scale. *Phys. Rev. Lett.* **98**, 021101 (2007)
71. Adelberger, E.G., Heckel, B.R., Hoedl, S., Hoyle, C.D., Kapner, D.J., Upadhye, A.: Particle-Physics Implications of a Recent Test of the Gravitational Inverse-Square Law. *Phys. Rev. Lett.* **98**, 131104 (2007)
72. Mostepanenko, V.M., Sokolov, I.Yu.: The Casimir effect leads to new restrictions on long-range force constants. *Phys. Lett. A* **125**, 405–408 (1987)
73. Derjaguin, B.V., Abrikosova, I.I., Lifshitz, E.M.: Direct measurement of molecular attraction between solids separated by a narrow gap. *Quat. Rev.* **10**, 295–329 (1956)
74. Feinberg, G., Sucher, J.: Is there a strong van der Waals between hadrons? *Phys. Rev. D* **20**, 1717–1724 (1979)
75. Tan, W.-H., Du, A.-B., Dong, W.-C., Yang, S.-Q., Shao, C.-G., Guan, S.-G., Wang, Q.-L., Zhan, B.-F., Luo, P.-S., Tu, L.-C., Luo, J.: Improvement for Testing the Gravitational Inverse-Square Law at the Submillimeter Range. *Phys. Rev. Lett.* **124**, 051301 (2020)
76. Dimopoulos, S., Giudice, G.F.: Macroscopic forces from supersymmetry. *Phys. Lett. B* **379**, 105–114 (1996)
77. Fujii, Y.: The theoretical background of the fifth force. *Int. J. Mod. Phys. A* **6**, 3505–3557 (1991)
78. Peccei, R.D., Quinn, H.R.: CP Conservation in the Presence of Pseudoparticles. *Phys. Rev. Lett.* **38**, 1440–1443 (1977)
79. Antoniadis, I., Arkani-Hamed, N., Dimopoulos, S., Dvali, G.: New dimensions at a millimeter to a fermi and superstrings at a TeV. *Phys. Lett. B* **436**, 257–263 (1998)
80. Arkani-Hamed, N., Dimopoulos, S., Dvali, G.: Phenomenology, astrophysics, and cosmology of theories with millimeter dimensions and TeV scale quantum gravity. *Phys. Rev. D* **59**, 086004 (1999)
81. Floratos, E.G., Leontaris, G.K.: Low scale unification, Newton's law and extra dimensions. *Phys. Lett. B* **465**, 95–100 (1999)
82. Kehagias, A., Sfetsos, K.: Deviations from  $1/r^2$  Newton law due to extra dimensions. *Phys. Lett. B* **472**, 39–44 (2000)
83. Fischbach, E., Talmadge, C.L.: *The Search for Non-Newtonian Gravity*. Springer-Verlag, New York (1999)
84. Smullin, S.J., Geraci, A.A., Weld, D.M., Chiaverini, J., Holmes, S., Kapitulnik, A.: Constraints on Yukawa-type deviations from Newtonian gravity at 20 microns. *Phys. Rev. D* **72**, 122001 (2005)

85. Hoskins, J.K., Newman, R.D., Spero, R., Schultz, J.: Experimental tests of the gravitational inverse-square law for mass separations from 2 to 105 cm. *Phys. Rev. D* **32**, 3084–3095 (1985)
86. Schlamminger, S., Choi, K.-J., Wagner, T.A., Gundlach, J.H., Adelberger, E.G.: Test of the Equivalence Principle Using a Rotating Torsion Balance. *Phys. Rev. Lett.* **100**, 041101 (2008)
87. Kuzmin, V.A., Tkachev, I.I., Shaposhnikov, M.E.: Restrictions imposed on light scalar particles by measurements of van der Waals forces. *Pis'ma v Zh. Eksp. Teor. Fiz.* **36**, 49–52 (1982); *JETP Lett.* **36**, 59–62 (1982)
88. Tabor, D., Winterton, R.H.S.: Surface Forces: Direct Measurement of Normal and Retarded van der Waals Forces. *Nature* **219**, 1120–1121 (1968)
89. Decca, R.S., Fischbach, E., Klimchitskaya, G.L., Krause, D.E., López, D., Mostepanenko, V.M.: Application of the proximity force approximation to gravitational and Yukawa-type forces. *Phys. Rev. D* **79**, 124021 (2009)
90. Chiu, H.C., Klimchitskaya, G.L., Marachevsky, V.N., Mostepanenko, V.M., Mohideen, U.: Demonstration of the asymmetric lateral Casimir force between corrugated surfaces in the nonadditive regime. *Phys. Rev. B* **80**, 121402(R) (2009)
91. Chiu, H.C., Klimchitskaya, G.L., Marachevsky, V.N., Mostepanenko, V.M., Mohideen, U.: Lateral Casimir force between sinusoidally corrugated surfaces: Asymmetric profiles, deviations from the proximity force approximation, and comparison with exact theory. *Phys. Rev. B* **81**, 115417 (2010)
92. Bezerra, V.B., Klimchitskaya, G.L., Mostepanenko, V.M., Romero, C.: Advance and prospects in constraining the Yukawa-type corrections to Newtonian gravity from the Casimir effect. *Phys. Rev. D* **81**, 055003 (2010)
93. Banishev, A.A., Wagner, J., Emig, T., Zandi, R., Mohideen, U.: Demonstration of Angle-Dependent Casimir Force between Corrugations. *Phys. Rev. Lett.* **110**, 250403 (2013)
94. Banishev, A.A., Wagner, J., Emig, T., Zandi, R., Mohideen, U.: Experimental and theoretical investigation of the angular dependence of the Casimir force between sinusoidally corrugated surfaces. *Phys. Rev. B* **89**, 235436 (2014)
95. Klimchitskaya, G.L., Mohideen, U., Mostepanenko, V.M.: Constraints on corrections to Newtonian gravity from two recent measurements of the Casimir interaction between metallic surfaces. *Phys. Rev. D* **87**, 125031 (2013)
96. Chen, Y.J., Tham, W.K., Krause, D.E., López, D., Fischbach, E., Decca, R.S.: Stronger Limits on Hypothetical Yukawa Interactions in the 30–8000 Nm Range. *Phys. Rev. Lett.* **116**, 221102 (2016)
97. Nesvizhevsky, V.V., Pignol, G., Protasov, K.V.: Neutron scattering and extra short range interactions. *Phys. Rev. D* **77**, 034020 (2008)
98. Kamiya, Y., Itagami, K., Tani, M., Kim, G.N., Komamiya, S.: Constraints on New Gravitylike Forces in the Nanometer Range. *Phys. Rev. Lett.* **114**, 161101 (2015)
99. Haddock, C.C., Oi, N., Hirota, K., Ino, T., Kitaguchi, M., Matsumoto, S., Mishima, K., Shima, T., Shimizu, H.M., Snow, W.M., Yoshioka, T.: Search for deviations from the inverse square law of gravity at nm range using a pulsed neutron beam. *Phys. Rev. D* **97**, 062002 (2018)
100. Mostepanenko, V.M., Novello, M.: Constraints on non-Newtonian gravity from the Casimir force measurements between two crossed cylinders. *Phys. Rev. D* **63**, 115003 (2001)
101. Masuda, M., Sasaki, M.: Limits on Nonstandard Forces in the Submicrometer Range. *Phys. Rev. Lett.* **102**, 171101 (2009)
102. Klimchitskaya, G.L., Mohideen, U., Mostepanenko, V.M.: Constraints on non-Newtonian gravity and light elementary particles from measurements of the Casimir force by means of a dynamic atomic microscope. *Phys. Rev. D* **86**, 065025 (2012)
103. Klimchitskaya, G.L., Kuusk, P., Mostepanenko, V.M.: Constraints on non-Newtonian gravity and axionlike particles from measuring the Casimir force in nanometer separation range. *Phys. Rev. D* **101**, 056013 (2020)
104. Klimchitskaya, G.L., Mostepanenko, V.M.: Dark Matter Axions, Non-Newtonian Gravity and Constraints on them from Recent Measurements of the Casimir Force in the Micrometer Separation Range. *Universe* **7**, 343 (2021)
105. Karshenboim, S.G.: Constraints on a long-range spin-independent interaction from precision atomic physics. *Phys. Rev. D* **82**, 073003 (2010)

106. Oort, J.H.: The force exerted by the stellar system in the direction perpendicular to the galactic plane and some related problems. *Bull. Astron. Inst. Neth.* **6**, 249–287 (1932)
107. Zwicky, F.: Die Rotverschiebung von extragalaktischen Nebeln. *Helv. Phys. Acta* **6**, 110–127 (1933)
108. Bertone, G., Hooper, D.: Hystory of Dark Matter. *Rev. Mod. Phys.* **90**, 045002 (2018)
109. Overduin, J.M., Wesson, P.S.: Dark Matter and Background Light. *Phys. Rep.* **402**, 267–406 (2004)
110. Bertone, G., Hooper, D., Silk, J.: Particle dark matter: Evidence, candidates and constraints. *Phys. Rep.* **405**, 279–390 (2005)
111. Sanders, R.H.: *The Dark Matter Problem: A Historical Perspective*. Cambridge University Press, Cambridge (2010)
112. Matarrese, S., Colpi, M., Gorini, V., Moshella, U. (Eds.): *Dark Matter and Dark Energy*. Springer, Dordrecht (2011)
113. Weinberg, S.: A New Light Boson? *Phys. Rev. Lett.* **40**, 223–226 (1978)
114. Wilczek, F.: Problem of Strong  $P$  and  $T$  Invariance in the Presence of Instantons. *Phys. Rev. Lett.* **40**, 279–283 (1978)
115. Kim, J.E.: Light pseudoscalars, particle physics and cosmology. *Phys. Rep.* **150**, 1–177 (1987)
116. Adelberger, E.G., Heckel, B.R., Stubbs, C.W., Rogers, W.F.: Searches for new Macroscopic forces. *Annu. Rev. Nucl. Part. Sci.* **41**, 269–320 (1991)
117. Rosenberg, L.J., van Bibber, K.A.: Searches for invisible axions. *Phys. Rep.* **325**, 1–39 (2000)
118. Raffelt, G.G.: Axions—Motivation, limits and searches. *J. Phys. A Math. Theor.* **40**, 6607–6620 (2007)
119. Kawasaki, M., Nakayama, K.: Axions: Theory and Cosmological Role. *Annu. Rev. Nucl. Part. Sci.* **63**, 69–95 (2013)
120. Ivastorza, I.G., Redondo, J.: New experimental approaches in the search for axion-like particles. *Progr. Part. Nucl. Phys.* **102**, 89–159 (2018)
121. Klimchitskaya, G.L.: Constraints on Theoretical Predictions beyond the Standard Model from the Casimir Effect and Some Other Tabletop Physics. *Universe* **7**, 47 (2021)
122. Peebles, P.J.E., Ratra, B.: The cosmological constant and dark energy. *Rev. Mod. Phys.* **75**, 559–606 (2003)
123. Weinberg, S.: The cosmological constant problem. *Rev. Mod. Phys.* **61**, 1–23 (1989)
124. Frieman, J.A., Turner, M.S., Huterer, D.: Dark Energy and the Accelerating Universe. *Annu. Rev. Astron. Astrophys.* **46**, 385–432 (2008)
125. Zel'dovich, Ya.B.: The cosmological constant and the theory of elementary particles. *Uspekhi Fiz. Nauk* **95**, 209–230 (1968); *Sov. Phys. Usp.* **11**, 381–393 (1968)
126. Adler, R.J., Casey, B., Jacob, O.C.: Vacuum catastrophe: An elementary exposition of the cosmological constant problem. *Amer. J. Phys.* **63**, 620–626 (1995)
127. Khoury, J., Weltman, A.: Chameleon cosmology. *Phys. Rev. D* **69**, 044026 (2004)
128. Olive, K.A., Pospelov, M.: Environmental dependence of masses and coupling constants. *Phys. Rev. D* **77**, 043524 (2008)
129. Hinterbichler, K., Khoury, J.: Screening Long-Range Forces through Local Symmetry Restoration. *Phys. Rev. Lett.* **104**, 231301 (2010)
130. Hinterbichler, K., Khoury, J., Levy, A., Matas, A.: Symmetron cosmology. *Phys. Rev. D* **84**, 103521 (2011)
131. Ryutov, D.D., Budker, D., Flambaum, V.V.: A Hypothetical Effect of the Maxwell-Proca Electromagnetic Stresses on Galaxy Rotation Curve. *ApJ* **871**, 218 (2019)
132. Gnedin, Y.N., Krasnikov, S.V.: Polarimetric effects associated with the detection of Goldstone bosons in stars and galaxies. *Sov. Phys. JETP* **75**, 933–937 (1992); *Zh. Eksp. Teor. Fiz.* **102**, 1729–1738 (1992)
133. Moody, J.E., Wilczek, F.: New macroscopic forces? *Phys. Rev. D* **30**, 130–139 (1984)
134. Bohr, A., Mottelson, B.R.: *Nuclear Structure, Volume 1*. Benjamin, New York (1969)
135. Adelberger, E.G., Fischbach, E., Krause, D.E., Newman, R.D.: Constraining the couplings of massive pseudoscalars using gravity and optical experiments. *Phys. Rev. D* **68**, 062002 (2003)

136. Ferrer, F., Nowakowski, M.: Higg- and Goldstone-boson-mediated long range forces. *Phys. Rev. D* **59**, 075009 (1999)
137. Drell, S.D., Huang, K.: Many-Body Forces and Nuclear Saturation. *Phys. Rev.* **91**, 1527–1543 (1953)
138. Aldaihan, S., Krause, D.E., Long, J.C., Snow, W.M.: Calculations of the dominant long-range, spin-independent contributions to the interaction energy between two nonrelativistic Dirac fermions from double-boson exchange of spin-0 and spin-1 bosons with spin-dependent couplings. *Phys. Rev. D* **95**, 096005 (2017).
139. Gradshtein, I.S., Ryzhik, I.M.: *Table of Integrals, Series and Products*. Academic Press, New York (1980)
140. Klimchitskaya, G.L., Mostepanenko, V.M.: Improved constraints on the coupling constants of axion-like particles to nucleons from recent Casimir-less experiment. *Eur. Phys. J. C* **75**, 164 (2015)
141. Ramsey, N.F.: The tensor force between two protons at long range. *Physica A* **96**, 285–289 (1979)
142. Ledbetter, M.P., Romalis, M.V., Jackson Kimball, D.F.: Constraints on Short-Range Spin-Dependent Interactions from Scalar Spin-Spin Coupling in Deuterated Molecular Hydrogen. *Phys. Rev. Lett.* **110**, 040402 (2013)
143. Long, J.C., Chan, H.W., Churnside, A.B., Gulbis, E.A., Varney, M.C.M., Price, J.C.: Upper limits to submillimetre-range forces from extra space-time dimensions. *Nature* **421**, 922–925 (2003)
144. Long, J.C., Kostelecký, V.A.: Search for Lorentz violation in short-range gravity. *Phys. Rev. D* **91**, 092003 (2015)
145. Vasilakis, G., Brown, J.M., Kornak, T.R., Romalis, M.V.: Limits on New Long Range Nuclear Spin-Dependent Forces Set with a  $K\text{-}^3\text{He}$  Comagnetometer. *Phys. Rev. Lett.* **103**, 261801 (2009)
146. Bezerra, V.B., Klimchitskaya, G.L., Mostepanenko, V.M., Romero, C.: Constraints on the parameters of an axion from measurements of the thermal Casimir-Polder force. *Phys. Rev. D* **89**, 035010 (2014)
147. Bezerra, V.B., Klimchitskaya, G.L., Mostepanenko, V.M., Romero, C.: Stronger constraints on an axion from measuring the Casimir interaction by means of a dynamic atomic force microscope. *Phys. Rev. D* **89**, 075002 (2014)
148. Bezerra, V.B., Klimchitskaya, G.L., Mostepanenko, V.M., Romero, C.: Constraining axion-nucleon coupling constants from measurements of effective Casimir pressure by means of micromachined oscillator. *Eur. Phys. J. C* **74**, 2859 (2014)
149. Bezerra, V.B., Klimchitskaya, G.L., Mostepanenko, V.M., Romero, C.: Constraints on axion-nucleon coupling constants from measuring the Casimir force between corrugated surfaces. *Phys. Rev. D* **90**, 055013 (2014)
150. Klimchitskaya, G.L., Mostepanenko, V.M.: Constraints on axionlike particles and non-Newtonian gravity from measuring the difference of Casimir forces. *Phys. Rev. D* **95**, 123013 (2017)
151. Mostepanenko, V.M., Klimchitskaya, G.L.: The State of the Art in Constraining Axion-to-Nucleon Coupling and Non-Newtonian Gravity from Laboratory Experiments. *Universe* **6**, 147 (2020)
152. Bezerra, V.B., Klimchitskaya, G.L., Mostepanenko, V.M., Romero, C.: Constraining axion coupling constants from measuring the Casimir interaction between polarized test bodies. *Phys. Rev. D* **94**, 035011 (2016)
153. Takyu, K., Itoh, K.M., Oka, K., Saito, N., Ozhogin, V.I.: Growth and Characterization of the Isotopically Enriched  $^{28}\text{Si}$  Bulk Single Crystal. *Jpn. J. Appl. Phys.* **38**, L1493 (1999)
154. Brax, P., van de Bruck, C., Davis, A.-C., Mota, D.F., Shaw, D.: Detecting chameleons through Casimir force measurements. *Phys. Rev. D* **76**, 124034 (2007)
155. Mota, D.F., Shaw, D.J.: Evading equivalence principle violations, cosmological, and experimental constraints in scalar field theories with a strong coupling to matter. *Phys. Rev. D* **75**, 063501 (2007)

156. Burrage, C., Sakstein, J.: Tests of chameleon gravity. *Living Rev. Relativ.* **21**, 1 (2018)
157. Elder, B., Vardanyan, V., Arkami, Y., Brax, P., Davis, A.-C., Decca, R.S.: Classical symmetron force in Casimir experiments. *Phys. Rev. D* **101**, 064065 (2020)
158. Klimchitskaya, G.L.: Recent breakthrough and outlook in constraining the non-Newtonian gravity and axion-like particles from Casimir physics. *Eur. Phys. J. C* **77**, 315 (2017)
159. Almasi, A., Brax, P., Iannuzzi, D., Sedmik, R.I.P.: Force sensor for chameleon and Casimir force experiments with parallel-plate configuration. *Phys. Rev. D* **91**, 102002 (2015)
160. Sedmik, R., Brax, P.: Status Report and first Light from Cannex: Casimir Force Measurements between flat parallel Plates. *J. Phys.: Conf. Ser.* **1138**, 012014 (2018)
161. Klimchitskaya, G.L., Mostepanenko, V.M., Sedmik, R.I.P., Abele, H.: Prospects for Searching Thermal Effects, Non-Newtonian Gravity and Axion-Like Particles: CANNEX Test of the Quantum Vacuum. *Symmetry* **11**, 407 (2019)
162. Klimchitskaya, G.L., Mostepanenko, V.M., Sedmik, R.I.P.: Casimir pressure between metallic plates out of thermal equilibrium: Proposed test for the relaxation properties of free electrons. *Phys. Rev. A* **100**, 022511 (2019)
163. Sedmik, R.I.P.: Casimir and non-Newtonian force experiment (CANNEX): Review, status, and outlook. *Int. J. Mod. Phys. A* **35**, 2040008 (2020)
164. Bennett, R., O'Dell, D.H.J.: Revealing short-range non-Newtonian gravity through Casimir-Polder shielding. *New J. Phys.* **21**, 033032 (2019)
165. Mattioli, L., Frassinio, A.M., Panella, O.: Casimir-Polder interactions with massive photons: Implications for BSM physics. *Phys. Rev. D* **100**, 116023 (2019)
166. Chen, L., Liu, J., Zhuy, K.: Constraining the axion-nucleon coupling and non-Newtonian gravity with a levitated optomechanical device. *Phys. Rev. D* **106**, 095007 (2022)
167. Haddock, C.C., Oi, N., Hirota, K., Ino, T., Takashi Ino, Kitaguchi, M., Matsumoto, S., Mishima, K., Shima, T., Shimizu, H.M., Snow, W.M., Yoshioka, T.: Search for deviations from the inverse square law of gravity at nm range using a pulsed neutron beam. *Phys. Rev. D* **97**, 062002 (2018)
168. Brax, P., Fichet, S., Pignol, G.: Bounding quantum dark forces. *Phys. Rev. D* **97**, 115034 (2018)
169. Sponar, S., Sedmik, R.I.P., Pitschmann, M., Abele, H., Hasegawa, Y.: Tests of fundamental quantum mechanics and dark interactions with low-energy neutrons. *Nature Rev. Phys.* **3**, 309–327 (2021)
170. Heacock, B., Fujiie, T., Haun R.W., Henins, A., Hirota, K., Hosobata, T., Huber, M.G., Kitaguchi, M., Pushin, D.A., Shimizu, H., Takeda, M., Valdillez, R., Yamagata, Y., Young A.: Pendellösung interferometry probes the neutron charge radius, lattice dynamics, and fifth forces. *Science* **373**, 1239–1243 (2021)
171. Rocha, J.M., Dahia, F.: Neutron interferometry and tests of short-range modifications of gravity. *Phys. Rev. D* **103**, 124014 (2021)
172. Borkowski, M., Buchachenko, A.A., Ciury lo, R., Julienne, P.S., Yamada, H., Kikuchi, Y., Takasu, Y., Takahashi, Y.: Weakly bound molecules as sensors of new gravitylike forces. *Sci. Rep.* **9**, 14807 (2019)
173. Hollik, W.G., Linster, M., Tabet, T.: A study of New Physics searches with tritium and similar molecules. *Eur. Phys. J. C* **80**, 661 (2020)
174. Lemos, A.S.: Submillimeter constraints for non-Newtonian gravity from spectroscopy. *Europhys. Lett.* **135**, 11001 (2021)
175. Hebestreit, E., Frimmer, M., Reimann, R., Novotny, L.: Sensing Static Forces with Free-Falling Nanoparticles. *Phys. Rev. Lett.* **121**, 063602 (2018)
176. Liu, J.; Zhu, K.-D.: Detecting large extra dimensions with optomechanical levitated sensors. *Eur. Phys. J. C* **79**, 18 (2019)
177. Ren, X., Wang, J., Luo, R., Yin, L., Ding, J., Zeng, G., Luo, P.: Search for an exotic parity-odd spin- and velocity-dependent interaction using a magnetic force microscope. *Phys. Rev. D* **104**, 032008 (2021)
178. Banks, H., McCullough, M.: Charting the fifth force landscape. *Phys. Rev. D* **103**, 075018 (2021)
179. Faizal, M., Patel, H.: Probing Short Distance Gravity using Temporal Lensing. *Int. J. Mod. Phys. A* **36**, 2150115 (2021)